Intriguing tetranuclear Rh-based polyoxometalate for the reduction of nitroarene and oxidation of aniline

Wenjing Chen, Huafeng Li, Yuzhen Jin, Che Wu, Zelong Yuan, Pengtao Ma, Jingping Wang * and Jingyang Niu *[a]

[a]Henan Key Laboratory of Polyoxometalate Chemistry, College of Chemistry and Chemical Engineering, Henan University, Kaifeng, Henan 475004, (P. R. China), Fax: (+86)-371-23886876, E-mail: jyniu@henu.edu.cn, jpwang@henu.edu.cn

Content:

Materials and Physical Measurements

All chemicals were purchased commercially without further purification. The precursor $K_{14}[As_2W_{19}O_{67}(H_2O)]$ (As_2W_{19}) was obtained from the literature and corroborated by IR spectroscopy. An Elementar VarioELcube CHNS analyzer was used to record the elemental analyses. Using KBr pellets, IR spectra in the range of 500–4000 cm^{-1} were collected on a Bruker VERTEX 70 IR spectrometer. The X-ray powder diffractometer (Bruker, D8 Advance) was used to record X-ray powder diffraction (PXRD) patterns in the 2θ angular range of 5−50° under Cu Kα radiation. The U-4100 spectrophotometer was used to measure UV/vis absorption spectra at room temperature. Thermogravimetric analyses (TGA) were carried out in a N_2 environment in the temperature range of 25 to 950 °C with a heating rate of 10 °C min^{-1} using a NETZSCH STA 449 F5 Jupiter thermal analyzer. For inductively coupled plasma-atomic emission spectrometry (ICP-AES) analyses (Na, Rh, As, and W), a Perkin Elmer Optima 2100 DV spectrometer was chosen. The X-ray photoelectron spectra (XPS) were recorded on a Thermo Scientific K-Alpha spectrometer with monochromatic Al (hν = 1486.6 eV) as the excitation source. The ABSCIEX triple-TOF 4600 mass spectrometer was used to perform electrospray ionization-mass spectrometry (ESI-MS). On a Bruker 450-GC with a flame ionization detector and a 30 m column with nitrogen as the carrier gas, GC-MS (Agilent 7890B GC/5973B MS, SE-54 capillary column) and GC analyses were performed. The Bruker AVANCE NEO 500 MHz NMR spectrometer was used to record ^1H and ^{13}C NMR spectra.

Syntheses of 1

As_2W_{19} was added to 10 ml of sodium acetate buffer solution (1 M, pH = 4.5) and stirred for 10 min. The mixed solution was adjusted to pH=2.6 with 12 M HCl, and then $RhCl_3{\cdot}3H_2O$ (0.1 g) and 2,1,3-Benzothiadiazole (0.05 g) were added, with the solution having a colorless change to red. After continuing stirring for 1 h the mixed solution was sealed in a 25 mL Teflon-lined autoclave and heated at 200°C for 72 h. Following cooling to room temperature, the solution was filtered and slowly evaporated. Yellow flaky crystal **1** was obtained after two weeks. Yield: 2.11% (0.015 g, based on Rh). Elemental analysis calcd (%) for **1**: Na, 1.05; As, 2.56; Rh, 4.97; W, 62.77; C, 5.33; H, 0.53; N, 1.91; S, 0.55. Found: Na, 1.20; As, 2.56; Rh, 5.02; W, 66.56; C, 4.19; H, 0.59; N, 1.86; S, 0.65. IR (KBr pellet, cm^{-1}): 3472 (br), 2925 (s), 1626 (s), 970 (s), 836 (s), 804 (s), 717 (s), 621 (s), 575 (s).

X-ray crystallography

On the Bruker D8 VENTURE PHOTON II CCD diffractometer, a yellow flaky crystal was chosen and put. The crystal data was collected using a graphite-monochromated Mo Kα (λ = 0.71073 Å) radiation source. The SHELXT structure solution program was used to solve all the structures, and the SHELXL refinement package in Olex2 was used for the full-matrix least-squares algorithm on F^2 data.[1,2] The C, N, O, S, As, Rh, W, Cl and Na atoms were refined into anisotropy in the final refinement cycle. The Fourier maps and TGA data validated the assignment of water molecules. Placing the hydrogen atoms from the organic ligands in the calculated position. Table S1 shows the crystallographic data and structural refinement parameters for **1**, with CCDC number: 2153638.

Catalytic cycle process

The products were all extracted with hexane. Add excess hexane to the reaction mother liquor (the ratio of mother liquor to hexane by volume is 1:10). The solution will be divided into two layers, with the upper layer being the hexane layer and the lower layer being the mother liquor layer (The color of mother liquor: yellow, in the reduction system; orange, in the oxidation system).[3] After shaking well, collect the bottom layer of mother liquor and discard the rest. The collected mother liquor will be concentrated on a rotary evaporator, and after concentration, the original volume of solvent will be added and used for the next cycle.

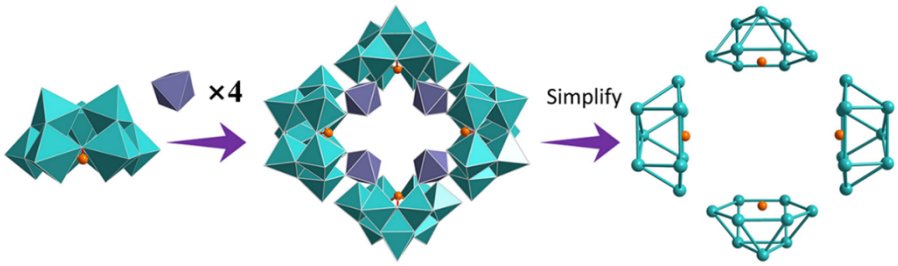

Fig. S1 Polyhedral combination demonstration and simplification of $\{As_4W_{40}\}$.

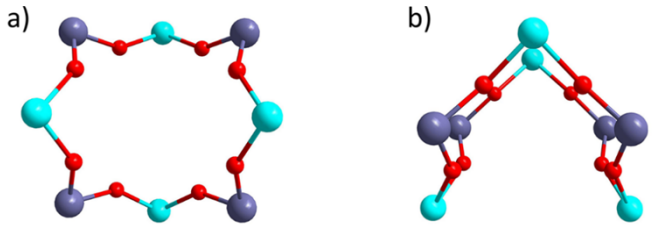

Fig. S2 Ball-and-stick representations of $\{Rh_4W_4\}$. a) view from the front; b) view from the side.

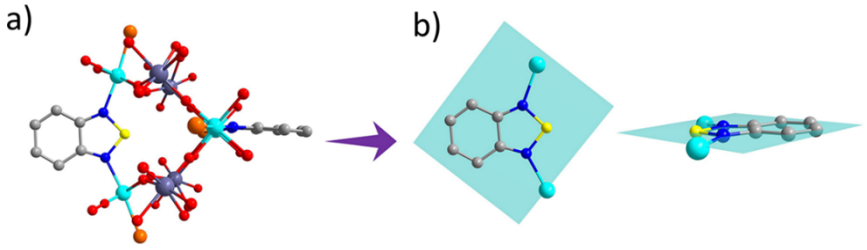

Fig. S3 (a) Orthogonal arrangement of two $Rh_2^{IV}(C_6H_4N_2S)^{8+}$ groups; (b) Simplify the display.

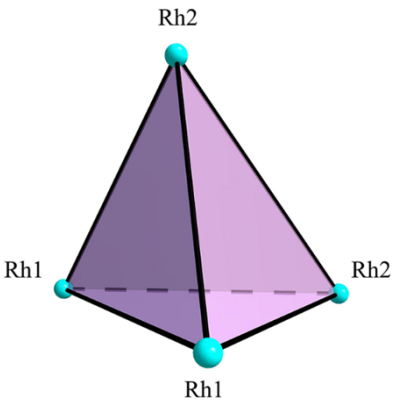

Fig. S4 The trigonal-pyramid geometry of the Rh atoms (Rh1 and Rh2).

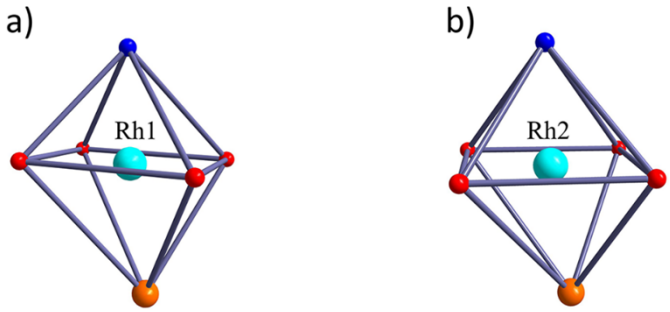

Fig. S5 The coordination geometries of (a) Rh1 in distorted octahedron; (b) Rh2 in distorted octahedron.

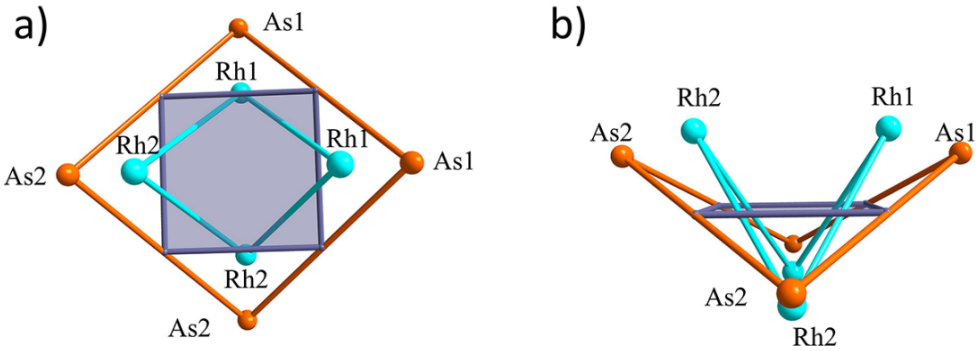

Fig. S6 The plane of W atoms. a) view from the front; b) view from the side.

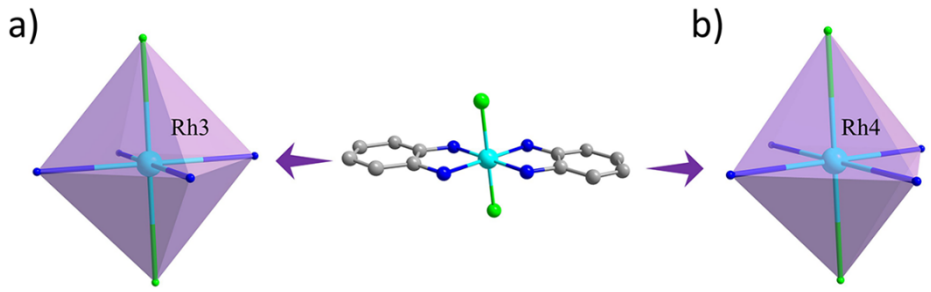

Fig. S7 The coordination geometries of (a) Rh3 in distorted octahedron; (b) Rh4 in distorted octahedron.

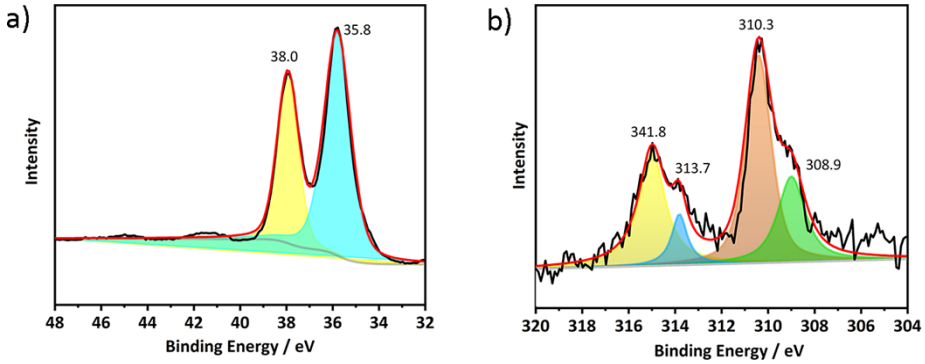

Fig. S8 The XPS spectra for the fresh catalyst: (a) W 4f, (b) Rh 3d. Spectra analysis was carried out using peak fitting with a Gaussian–Lorentzian peak shape and Shirley type background subtraction, and the C 1s peak typically located at 284.6 eV is used as a reference.

XPS Analyses

To further verify the valence state properties of **1**, the XPS spectra of Rh 3d and W 4f were recorded of the freshly prepared compound **1**, where the XPS peak value of W 4f was measured as ~35.8 and 38.0 eV, corresponding to the binding energy of W^{VI}.[4,5] In addition, the Rh 3d spectra presented peaks at 314.8 and 310.3 eV, attributed to the binding energies of Rh $3d_{3/2}$ and Rh $3d_{5/2}$ of Rh^{IV}.[6,7] The Rh 3d spectra presented peaks at 313.7 and 308.9 eV, attributed to the binding energies of Rh $3d_{3/2}$ and Rh $3d_{5/2}$ of Rh^{III}.[8,9] Thus, Rh1 and Rh2 are tetravalent and Rh3 and Rh4 are trivalent. The XPS analysis results are consistent the BVS (Table S4, ESI†).

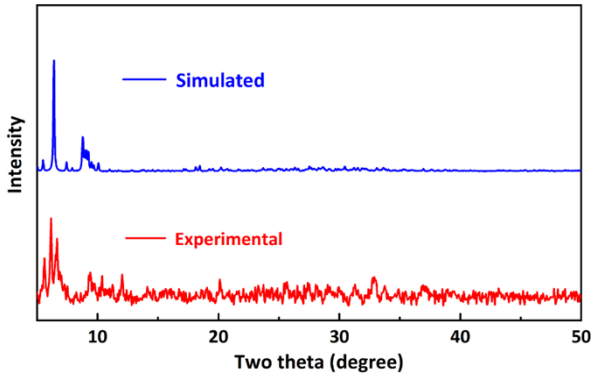

Fig. S9 PXRD patterns of **1**.

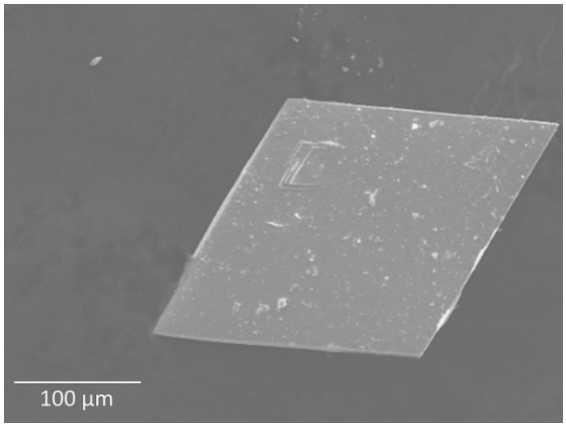

Fig. S10 SEM image for **1**.

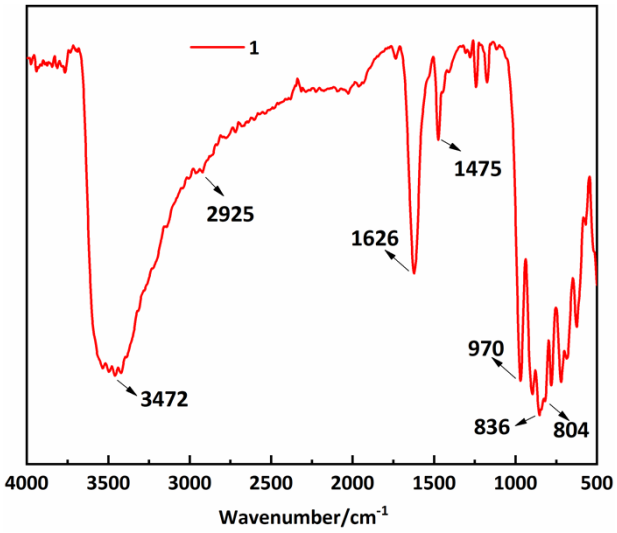

Fig. S11 The IR spectra of **1**.

The IR spectra of **1** were recorded with KBr particles at the range of 500-4000 cm^{-1}, corresponding to the characteristic vibration mode of keggin-type skeleton in the range of 1000-650 cm^{-1}. The characteristic vibration absorption band at λ = 970 cm^{-1} belongs to W–O_t vibration, while the *ν*(W-O_b-W) and *ν*(W-O_c-W) vibration bands are about 883 cm^{-1} and 804 cm^{-1} (O_t = terminal oxygen, O_b = bridged oxygen of two octahedrons sharing a corner, O_c = bridged oxygen connecting different octahedrons in the same group of three metal clusters), respectively.[10,11] The peak at 836 cm^{-1} can be attributed to As-O vibration.[12,13] Additionally, the vibration peaks observed at 3472 and 1626 cm^{-1} are ascribed to the vibration of lattice water molecules.[14] The weak band at around 2925 cm^{-1} comes from the C–H stretching vibration.[15,16]

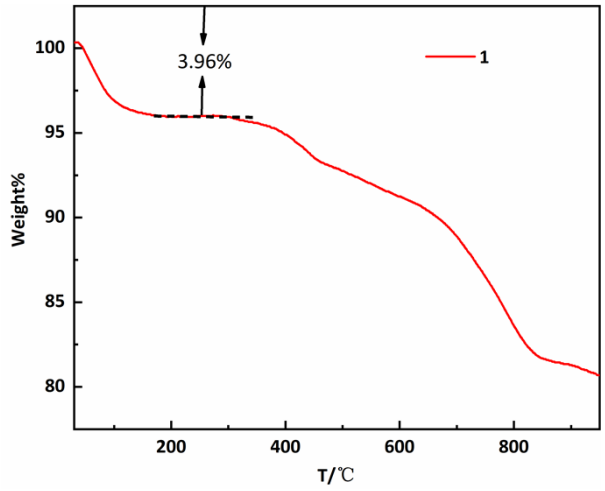

Fig. S12 Thermogravimetric curve of **1**.

Thermogravimetric Analyses.

The weight changes of **1** at programmed heating (10 °C/min) were measured in a temperature range of 25 °C to 950°C in N_2 atmosphere. As shown in Figure S6, compound **1** exhibits two-step weightlessness at 25–950°C. The weightlessness of 3.96% (25–250 °C) in the first step is the result of the loss of crystalline water molecules. In the second step, weight loss occurred in the range of 250–950 °C with a weight loss of 14.91%, corresponding to the decomposition of POM skeleton and the oxidation of ligands.[17]

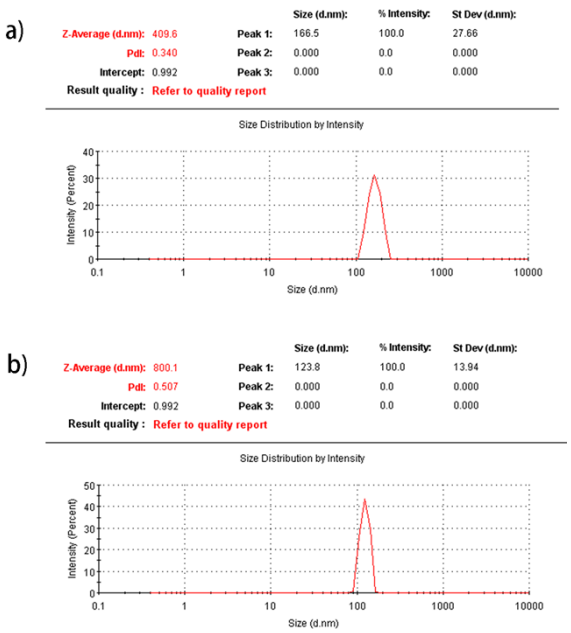

Fig. S13 Size distribution of **1** by Dynamic light scattering (DLS) at a concentration of 1 μM. a) in the nitrobenzene reduction catalytic system, b) in the oxidation of aniline catalytic system.

DLS measurements were performed on the catalytic systems containing **1** and **2**, and the results showed that one nanoparticle was detected, respectively, indicating that **1** and **2** were homogeneous in the catalytic system.[18,19] In addition, the formation of 100-200 nm nanoparticles indicates that **1** and **2** are aggregated in the catalytic system, which is not uncommon.[20]

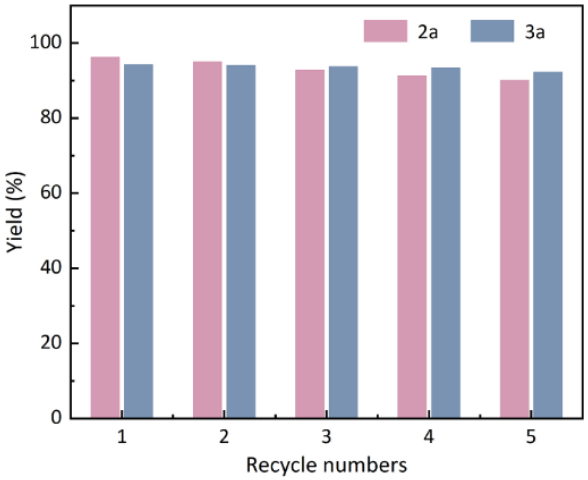

Fig. S14 Recycling experiments of **1** for reduction of nitroarene and oxidation of aniline.

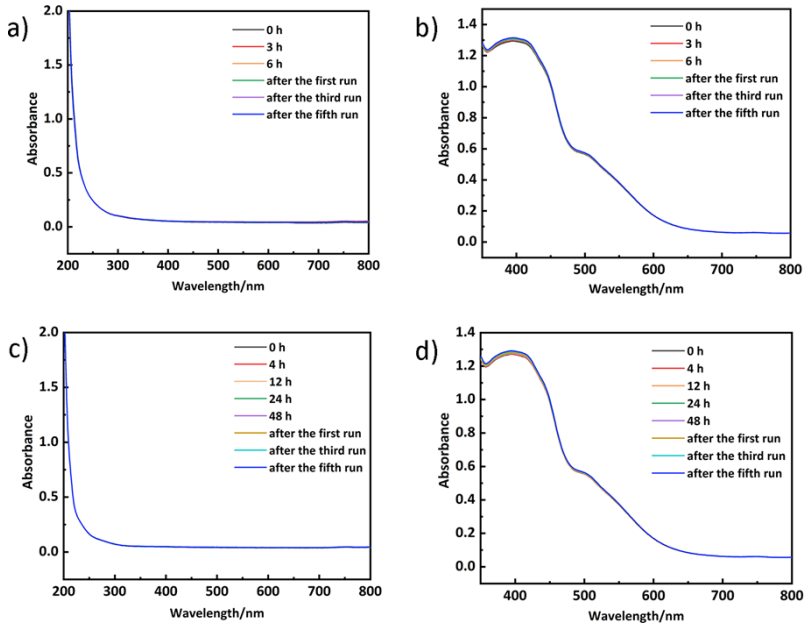

Fig. S15 Time-dependent UV-Vis spectra of **1** in the nitrobenzene reduction catalytic system, a) 1.0×10^{-6} M, b) 1.0×10^{-4} M. Time-dependent UV-Vis spectra of **1** in the oxidation of aniline catalytic system, c) 1.0×10^{-6} M, d) 1.0×10^{-4} M.

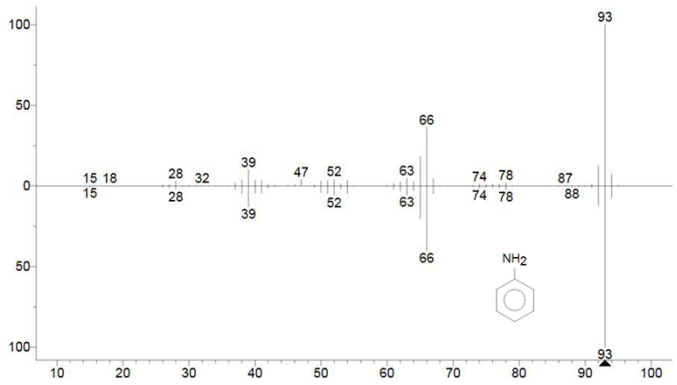

Fig. S16 The GC-MS spectrum of aniline. (bottom, simulation; top, experiment)

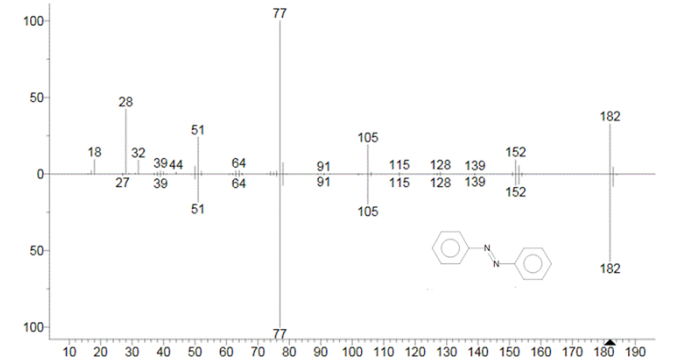

Fig. S17 The GC-MS spectrum of azobenzene. (bottom, simulation; top, experiment)

The mechanism research of nitrobenzene reduction.

There are currently two reaction pathways for the reduction of nitrobenzene to the corresponding aniline: direct and condensation. The direct reaction pathway is the formation of nitrosobenzene from nitrobenzene, followed by N-phenylhydroxylamine, and finally the reduction of N-phenylhydroxylamine to aniline; while the condensation route involves azobenzene intermediates (e.g., azoxybenzene and azobenzene).[21,22] Under visible light irradiation, the valence band (VB) of **1** occurs charge separation and electrons are transferred from the VB to the conduction band (CB), where holes are generated in the VB.[23] $N_2H_4 \cdot H_2O$ traps holes and generates protons, while photogenerated electrons may complete the whole photocatalytic cycle by hydrogenating nitrobenzene to produce aniline through different intermediates.[24,25] To clarify the possible mechanism of the nitrobenzene reduction reaction, some experiments were designed. The presence of aniline could be detected by GC-MS under optimized conditions with nitrosobenzene and N-phenylhydroxylamine as substrates (Fig. S16, ESI†). And when the intermediate azobenzene in the condensation route was used as a substrate, it showed no aniline. These results suggest that the nitrobenzene can be directly reduced to the corresponding aniline in this catalytic system.

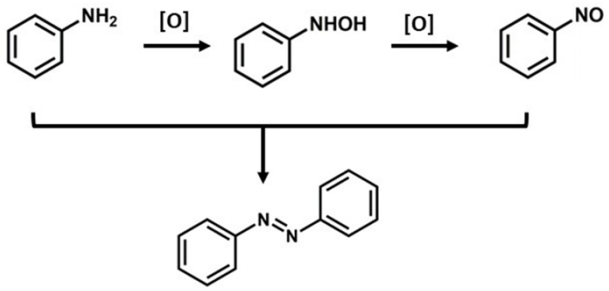

Scheme S1. The reaction pathway of aniline oxidation.

The oxidation of aniline is usually considered to proceed by two known mechanisms, namely the nitrosobenzene intermediate mechanism as well as the aniline radical mechanism.[26] In order to gain insight into the aniline oxidation process, several experiments were carried out. Aniline and nitrosobenzene were added to the same catalytic system, resulting in the detection of the azobenzene product (Fig. S17, ESI†). In addition, the addition of radical scavenger 6-di-tert-butyl-4-methylphenol (BHT) agent to the substrate aniline had no significant effect on the reaction, indicating that the reaction does not proceed through a radical process (Table 3, entry 9).[27] Therefore, we conclude that the catalytic reaction follows a nitrosobenzene intermediate mechanism.

Table S1 Crystallographic Data Parameters for **1**.

compound	**1**
empirical formula	C52H56As4Cl4N16Na5.34O146Rh5.66S2W40
formula weight	11805.96
temperature (K)	296.3
crystal system	monoclinic
space group	C2/c
a /Å	41.050(5)
b /Å	19.763(2)
c /Å	29.763(4)
β /deg	110.885(5)
V /Å^3	22559(5)
Z	4
ρ_{calc} /g cm^{-3}	3.476
μ /mm^{-1}	21.447
2ϑ range/deg	4.374 to 50.2
index ranges	-48 ≤ h ≤ 48, -23 ≤ k ≤ 23, -33 ≤ l ≤ 35
Reflections collected	84416
Independent reflections	20002
data/restraints/parameters	20002/36/1245
GOF on F^2	1.049
R_1, [a] wR_2 [b] [$I > 2\sigma(I)$]	0.0402, 0.0987
R_1, [a] wR_2 [b] [all data]	0.0579, 0.1101

[a] $R_1 = \sum||F_o| - |F_c||/\sum|F_o|$. [b] $wR_2 = [\sum w(F_o^2 - F_c^2)^2/\sum w(F_o^2)^2]^{1/2}$; $w = 1/[\sigma^2(F_o^2)+(xP)^2 + yP]$

Table S2 Selected bond distances (Å) for polyanion **1a**.

Bond	Length (Å)	Bond	Length (Å)	Bond	Length (Å)
Rh1–As1	2.404(17)	Rh1–N1	2.080(10)	Rh1–O15	2.007(9)
Rh1–O20	1.995(8)	Rh1–O24	2.013(9)	Rh1–O37	2.016(9)
Rh2–O39	2.006(9)	Rh2–O40	1.992(8)	Rh2–O46	2.010(9)
Rh2–O62	2.021(8)	Rh2–As2	2.4010(17)	Rh2–N2	2.084(11)
Rh3–Cl1	2.329(4)	Rh3–N5	2.104(13)	Rh3–N6	2.060(13)
Rh3–Cl1	2.329(4)	Rh3–N5	2.104(13)	Rh3–N6	2.060(13)
Rh4–Cl2	2.329(6)	Rh4–N3	2.064(13)	Rh4–N4	2.078(15)
Rh4–Cl2	2.329(6)	Rh4–N3	2.064(13)	Rh4–N4	2.078(15)
As1–O12	1.737(8)	As1–O14	1.751(9)	As1–O22	1.724(8)
As2–O2	1.740(8)	As2–O52	1.743(10)	As2–O53	1.712(9)
W1–O2	2.282(9)	W1–O62	1.813(8)	W1–O63	1.916(10)
W1–O64	1.719(10)	W1–O65	1.968(9)	W1–O66	1.991(10)
W2–O2	2.461(9)	W2–O50	1.817(9)	W2–O58	1.952(9)
W2–O65	1.920(9)	W2–O67	1.738(10)	W2–O68	2.000(9)
W3–O46	1.782(9)	W3–O50	2.020(9)	W3–O51	1.947(9)
W3–O46	1.782(9)	W3–O50	2.020(9)	W3–O51	1.947(9)
W4–O38	1.723(10)	W4–O39	1.836(9)	W4–O45	1.962(10)
W4–O52	2.268(9)	W4–O61	2.009(9)	W4–O63	1.940(9)
W5–O1	1.722(11)	W5–O41	1.797(10)	W5–O43	1.936(9)
W5–O45	1.898(10)	W5–O52	2.477(9)	W5–O54	1.977(9)

Table S3 Selected bond angle (°) for polyanion **1a**.

Bond	Angle (°)	Bond	Angle (°)	Bond	Angle (°)
N1–Rh1–As1	174.4(3)	O15–Rh1–As1	84.6(3)	O15–Rh1–N1	92.2(4)
O15–Rh1–O24	176.6(4)	O15–Rh1–O37	83.4(4)	O20–Rh1–As1	99.2(3)
O20–Rh1–N1	85.7(4)	O20–Rh1–O15	96.0(4)	O20–Rh1–O24	83.5(4)
O24–Rh1–As1	98.7(2)	O24–Rh1–N1	84.5(4)	O37–Rh1–As1	84.9(3)
O39–Rh2–As2	173.7(3)	O39–Rh2–N2	90.0(4)	O39–Rh2–O46	176.8(4)
N2–Rh2–As2	173.7(3)	O39–Rh2–O62	84.5(4)	O40–Rh2–As2	98.4(3)
O40–Rh2–N2	85.9(4)	O40–Rh2–O46	83.9(4)	O40–Rh2–O62	177.1(4)
O46–Rh2–As2	98.2(3)	O46–Rh2–N2	86.8(4)	O46–Rh2–O62	95.3(4)
N5–Rh3–Cl1	90.3(4)	N6–Rh3–Cl1	88.9(4)	N6–Rh3–N5	84.1(5)
N6–Rh3–N6	180	Cl2–Rh4–Cl2	180.0(3)	N3–Rh4–Cl2	91.0(4)
N3–Rh4–N3	180	N4–Rh4–Cl2	91.8(5)	N3–Rh4–Cl2	89.0(4)
O12–As1–O14	104.9(4)	O12–As1–Rh1	105.4(3)	O14–As1–Rh1	105.7(3)
O22–As1–O12	99.3(4)	O22–As1–O14	99.4(4)	O22–As1–Rh1	138.6(3)
O2–As2–O52	104.4(4)	O2–As2–Rh2	105.9(3)	O52–As2–Rh2	105.5(3)
O53–As2–O2	98.3(4)	O53–As2–O52	99.8(5)	O53–As2–Rh2	138.9(3)

Table S4 Bond valence sum (BVS) calculations of Rh, As, W and O atoms in **1a**.

Atom	BVS	Atom	BVS	Atom	BVS	Atom	BVS
Rh1	3.646	Rh2	3.652	Rh3	2.994	Rh4	2.994
As1	2.539	As2	2.586	W1	6.098	W2	5.863
W3	6.239	W4	5.926	W5	6.150	W6	6.121
W7	6.076	W8	6.047	W9	6.134	W10	6.044
W11	6.125	W12	6.034	W13	6.231	W14	5.993
W15	5.891	W16	6.152	W17	5.949	W18	6.257
W19	6.161	W20	6.009	W21	6.228	O1	1.694
O2	2.028	O3	1.745	O4	1.878	O5	1.788
O6	1.976	O7	1.953	O8	1.685	O9	1.824
O10	1.658	O11	1.963	O12	2.028	O13	1.978
O14	2.014	O15	1.871	O16	1.917	O17	1.909
O18	2.072	O19	1.980	O20	1.904	O21	1.948
O22	2.054	O23	1.967	O24	1.984	O25	1.991
O26	1.953	O27	1.769	O28	1.948	O29	1.822
O30	1.778	O31	2.061	O32	1.878	O33	1.689
O34	1.986	O35	1.868	O36	1.689	O37	1.868
O38	1.689	O39	2.031	O40	2.185	O41	2.079
O42	1.955	O43	1.989	O44	1.793	O45	1.938
O46	1.997	O47	1.822	O48	1.898	O49	2.035
O50	2.067	O51	1.969	O52	2.023	O53	2.072
O54	1.944	O55	1.941	O56	1.996	O57	1.803
O58	1.943	O59	1.717	O60	2.011	O61	1.835
O62	1.865	O63	1.942	O64	1.708	O65	1.863
O66	1.869	O67	1.622	O68	1.889	O69	1.722
O70	2.060						

Table S5 Optimization of **1** for reduction of nitrobenzene to aniline **2a** [a]

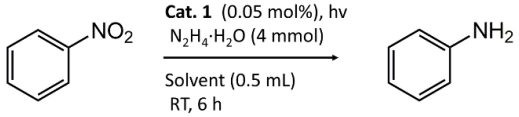

2a

Entry	Catalyst (mol%)	Solvent	Yield **2a** (%) [b]
1	**0.05**	**methanol**	**96.2**
2	0.05	CH_3CN	60.7
3	0.05	isopropyl alcohol	46.8
4	0.05	CH_2Cl_2	67.8
5	0.025	methanol	74.6
6	0.10	methanol	91.9
7 [c]	0.05	methanol	92.8

[a] **1** (0.05 mol%), substrate (0.5 mmol), methanol (0.5 mL), $N_2H_4·H_2O$ (4 mmol), N_2 (1 atm), 10 W LED lamp, RT, 6 h.
[b] Determined by GC analysis. [c] t=12 h.

Table S6 Effect of the amount of catalyst and additive on the yields of azobenzene **3a** [a]

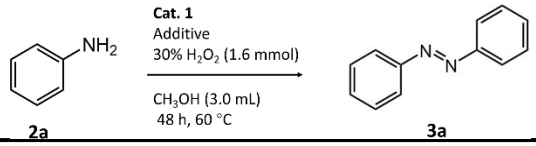

2a **3a**

Entry	Catalyst (mol%)	Additive (mmol)	Yield **3a** (%) [b]
1	0.05	–	67.5
2	0.05	K_2CO_3 (0.08)	Trace
3	0.05	$NaHCO_3$ (0.08)	46.2
4	0.05	K_3PO_4 (0.08)	Trace
5	0.05	As_2O_3 (0.08)	55.8
6	0.05	$NaAsO_2$ (0.08)	67.8
7	0.05	Na_2HAsO_4 (0.08)	50.0
8	0.05	Na_2SO_3 (0.08)	44.6
9	0.05	Na_2SO_4 (0.08)	38.6
10	0.05	$Na_2S_2O_4$ (0.08)	26.5
11	**0.05**	**$Na_2S_2O_8$ (0.08)**	**94.7**
12	0.05	$Na_2S_2O_8$ (0.04)	85.1
13	0.05	$Na_2S_2O_8$ (0.16)	89.9
14	0.03	$Na_2S_2O_8$ (0.08)	83.7
15	0.01	$Na_2S_2O_8$ (0.08)	72.2

[a] **1** (0.05 mol%), substrate (1.0 mmol), methanol (3.0 mL), 30% H_2O_2 (1.6 mmol), $Na_2S_2O_8$ (0.08 mmol), 60 °C, 48 h. [b] Yields determined by GC analysis.

Table S7 Effect of temperature, solvent and time on the yields of azobenzene **3a** [a]

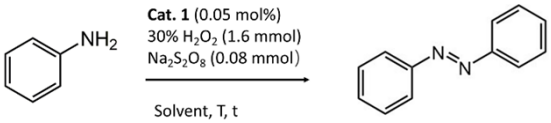

2a **3a**

Entry	T (°C)	Solvent (3.0 mL)	Time (h)	Yield **3a** (%) [b]
1	RT	CH_3OH	48	71.4
2	50	CH_3OH	48	84.1
3	**60**	**CH_3OH**	**48**	**94.7**
4	70	CH_3OH	48	90.3
5	60	H_2O	48	Trace
6	60	CH_3CN	48	69.7
7	60	DMF	48	17.1
8	60	CH_2Cl_2	48	45.3
9	60	MTBE	48	42.7
10	60	CH_3CH_2OH	48	40.5
11	60	CH_3OH	36	87.9
12	60	CH_3OH	24	79.4

[a] **1** (0.05 mol%), substrate (1.0 mmol), 30% H_2O_2 (1.6 mmol), $Na_2S_2O_8$ (0.08 mmol), 60 °C, 48 h. [b] Yields determined by GC analysis.

Table S8 Catalytic oxidation of aniline derivatives to azobenzenes by **1**[a, b]

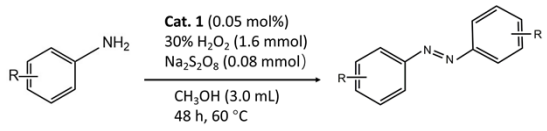

2 **3**

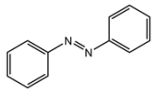 **3a**, 89.5%	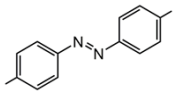 **3b**, 78.5%	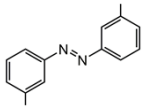 **3c**, 76.9 %
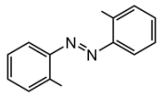 **3d**, 74.4%	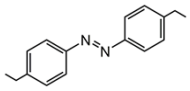 **3e**, 79.4%	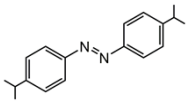 **3f**, 82.5%
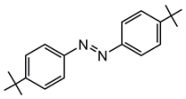 **3g**, 80.5%	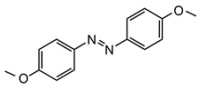 **3h**, 83.1%	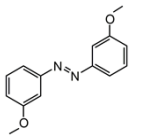 **3i**, 73.3%
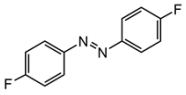 **3j**, 83.8%	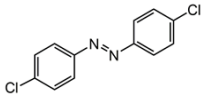 **3k**, 87.3%	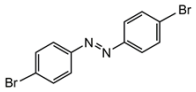 **3l**, 85.6%
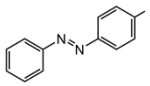 **3m**, 71.5%	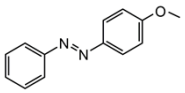 **3n**, 80.4%	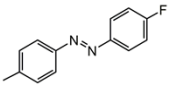 **3o**, 74.8%

[a] **1** (0.05 mol%), substrate (1.0 mmol), methanol (3.0 mL), 30% H_2O_2 (1.6 mmol), $Na_2S_2O_8$ (0.08 mmol), 60 °C, 48 h. [b] isolated yields.

Table S9 Summary of the yield of the reduction of nitrobenzene with different catalysts.

Entry	Catalyst	Temperature/°C	Light source	Hydrogen source	Time/h	Yield/%	Ref.
1	$Na_5H_{5.68}[NA_{0.17}Rh_{0.83}^{III}(C_6H_8N_2)_2Cl_2]_2(C_8H_8N_2)_2[As_4W_{40}O_{140}Rh_4^{IV}(C_6H_4N_2S)_2]\cdot nH_2O$	RT	Visiable light	$N_2H_4\cdot H_2O$	6	96	this work
2	CoW-TPT	RT	365 nm	TEOA	12	95	S28
3	Pd/C	80	/	$N_2H_4\cdot H_2O$	4	100	S29
4	Pd-Au NRs	25	λ> 320 nm	HCOOH/HCOONa	5	>99	S30
5	$PbBiO_2Br$	RT	440 nm	TEOA	6	>99	S31
6	Zr_{12}-TPDC-Co	110	/	$NaBEt_3H$/H_2	72	100	S32
7	Cu-$CoFe_2O_4$	RT	Visiable light	H_2O	1.5	99	S33
8	NC-90	90	/	$N_2H_4\cdot H_2O$	1	100	S34
9	MMC-Fe_2O_3	80	/	$N_2H_4\cdot H_2O$	2	100	S35
10	Rh-Fe_2O_3	80	/	$N_2H_4\cdot H_2O$	1	99	S36
11	Ag-rGO/g-C_3N_4	TR	λ> 400 nm	methanol	4	98	S23
12	3.0 wt% CQDs/$ZnIn_2S_4$	/	LED irradiation	TEOA/MeOH (1:1)	16	>99	S35
13	EY	RT	LED (525	TEOA	24	>99	S37

			nm)				
14	Co@CN/SiO_2-500	70	/	$N_2H_4 \cdot H_2O$	1.2	>99.5	S21

Table S10 Summary of the yield of the oxidation of aniline to azobenzene with different catalysts.

Entry	Catalyst	Temperature/°C	oxidant	Additive	Solvent	Time/h	Yield/%	Ref.
1	$Na_5H_{5.68}[NA_{0.17}Rh_{0.83}^{III}(C_6H_8N_2)_2Cl_2]_2(C_8H_8N_2)_2[As_4W_{40}O_{140}Rh_4^{IV}(C_6H_4N_2S)_2]\cdot nH_2O$	60	H_2O_2	$Na_2S_2O_8$	methanol	48	95	this work
2	$[N(C_4H_9)_4]_2[Mo_6O_{19}]$	60	H_2O_2	$Na_2S_2O_3$	methanol	24	99	S27
3	$Zr(OH)_4$	40	TBHP	/	acetic acid	24	90	S37
4	CuBr	60	air	pyridine	toluene	20	96	S38
5	meso-Mn_2O_3	110	air balloon	/	toluene	8	>99	S39
6	1.5% Au/TiO_2	100	O_2	/	toluene	22	99	S40
7	RuO_2/Cu_2O NPs	85	open atmosphere	/	MeCN	16	94	S41
8	Ag/C	60	air	/	DMSO	24	97	S42
9	Au_1Pd_3@C	333 K	O_2 balloon	/	DMSO	12	97	S43

Table S11 Assignment of peaks in negative mode mass spectra of after catalysis of **1**.

formula	m/z value		Simulation of peaks
	Observed	Theoretical	
$\{Na_5AsW_{40}O_{140}Rh_4^{IV}(C_6H_4N_2S)_2(H_2O)_{14}\}^{7-}$	1531.93	1531.38	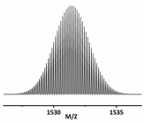
$\{Na_2H_4AsW_{40}O_{140}Rh_4^{IV}(C_6H_4N_2S)_2(H_2O)_{24}\}^{6-}$	1805.92	1805.81	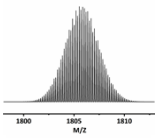
$\{Na_2H_4AsW_{40}O_{140}Rh_4^{IV}(C_6H_4N_2S)_2(H_2O)_{36}\}^{6-}$	1841.89	1841.84	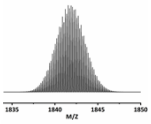
$\{Na_5H_2AsW_{40}O_{140}Rh_4^{IV}(C_6H_4N_2S)_2(H_2O)_{35}\}^{5-}$	2220.07	2220.00	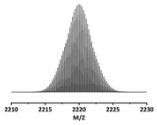
$\{Na_2H_5AsW_{40}O_{140}Rh_4^{IV}(C_6H_4N_2S)_2(H_2O)_{56}\}^{5-}$	2282.06	2282.47	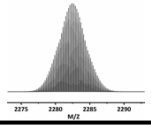

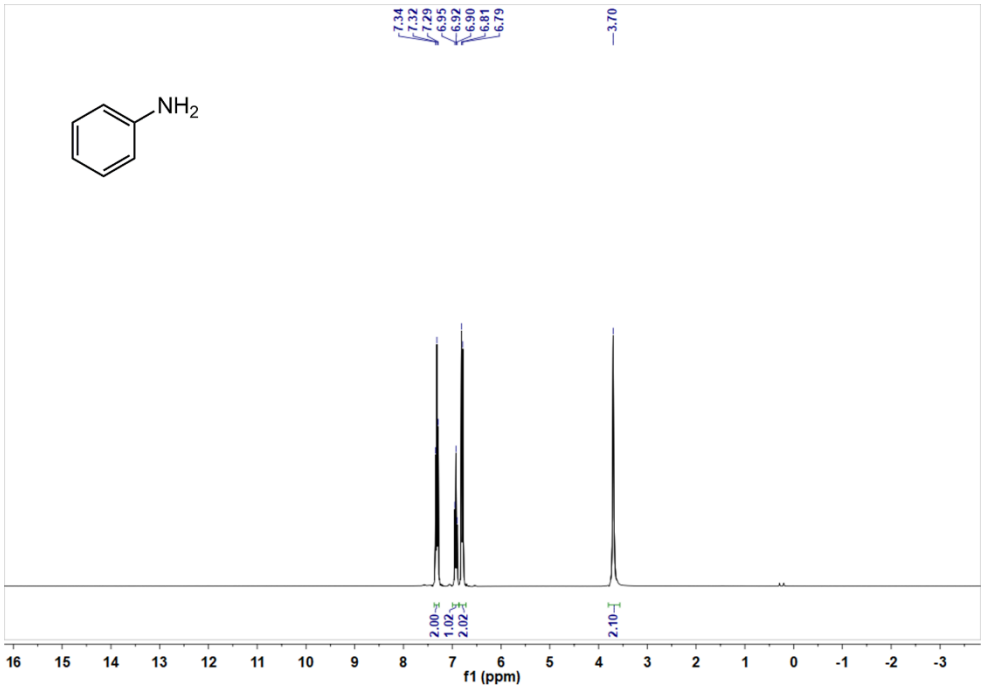

Fig. S18 ^{1}H NMR spectra of **2a** (500 MHz, $CDCl_3$).

Aniline(2a): ^{1}H NMR (500 MHz, $CDCl_3$) δ 7.32 (t, J = 7.8 Hz, 2H), 6.92 (t, J = 7.3 Hz, 1H), 6.80 (d, J = 7.5 Hz, 2H), 3.70 (s, 2H).

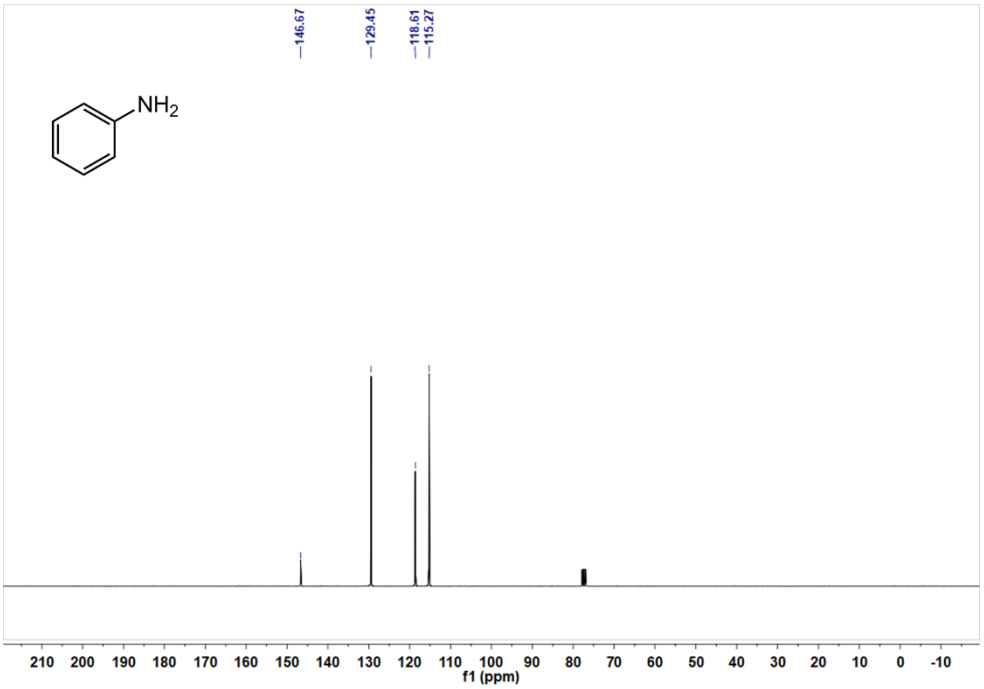

Fig. S19 ^{13}C NMR spectra of **2a** (126 MHz, $CDCl_3$).

Aniline(2a): ^{13}C NMR (126 MHz, $CDCl_3$) δ 146.67 (s), 129.45 (s), 118.61 (s), 115.27 (s).

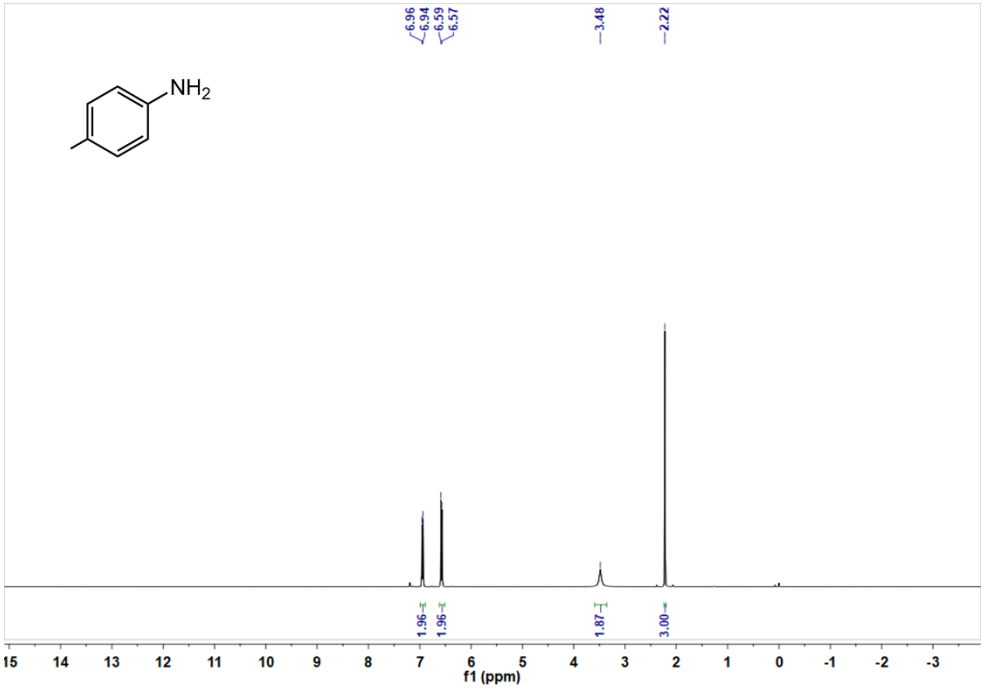

Fig. S20 ^{1}H NMR spectra of **2b** (500 MHz, $CDCl_3$).

p-Toluidine (2b): ^{1}H NMR (500 MHz, $CDCl_3$) δ 6.95 (d, J = 8.0 Hz, 2H), 6.58 (d, J = 8.3 Hz, 2H), 3.48 (s, 2H), 2.22 (s, 3H).

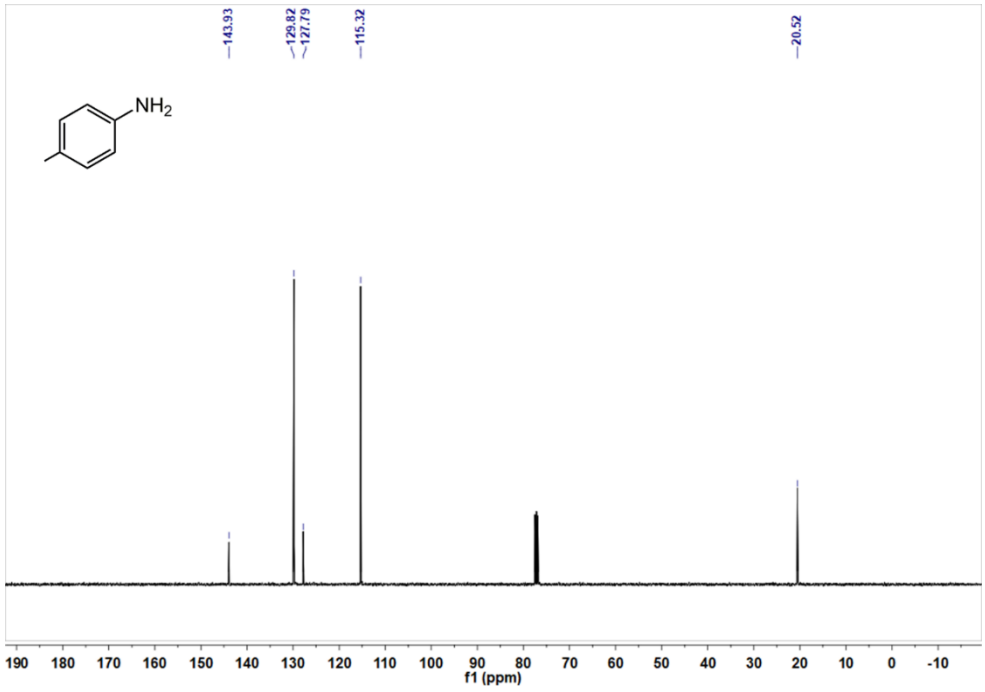

Fig. S21 ^{13}C NMR spectra of **2b** (126 MHz, $CDCl_3$).

p-Toluidine (2b): ^{13}C NMR (126 MHz, $CDCl_3$) δ 143.93 (s), 129.82 (s), 127.79 (s), 115.32 (s), 20.52 (s).

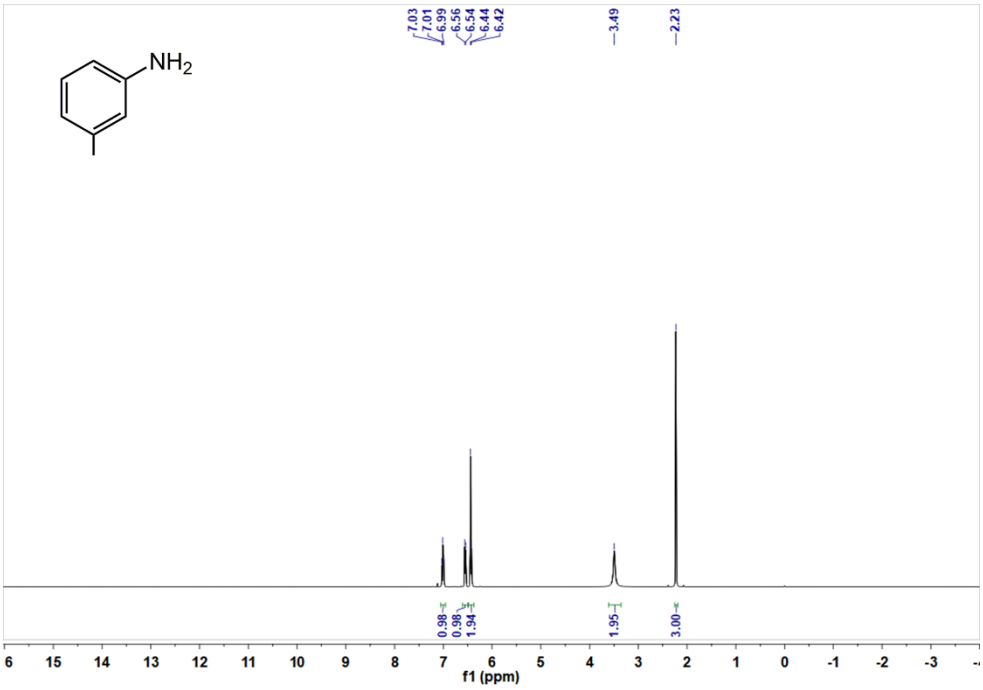

Fig. S22 ^{1}H NMR spectra of **2c** (500 MHz, $CDCl_3$).

m-Toluidine (2c): 1H NMR (500 MHz, $CDCl_3$) δ 7.01 (t, J = 7.4 Hz, 1H), 6.55 (d, J = 7.3 Hz, 1H), 6.43 (d, J = 7.4 Hz, 2H), 3.49 (s, 2H), 2.23 (s, 3H).

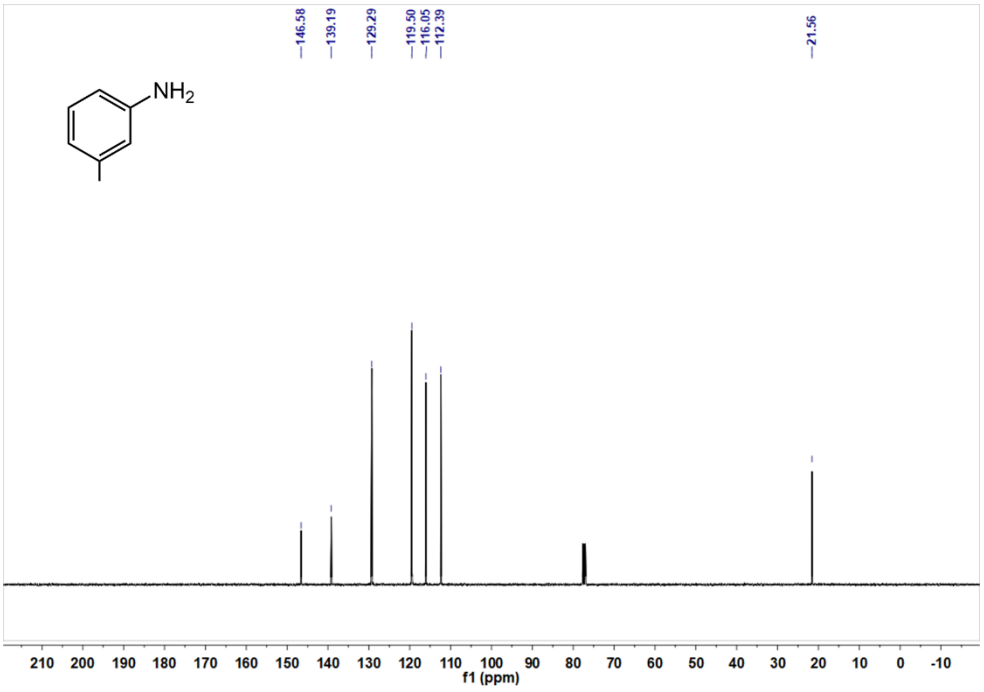

Fig. S23 ^{13}C NMR spectra of **2c** (126 MHz, $CDCl_3$).

m-Toluidine (2c): ^{13}C NMR (126 MHz, $CDCl_3$) δ 146.58 (s), 139.19 (s), 129.29 (s), 119.50 (s), 116.05 (s), 112.39 (s), 21.56 (s).

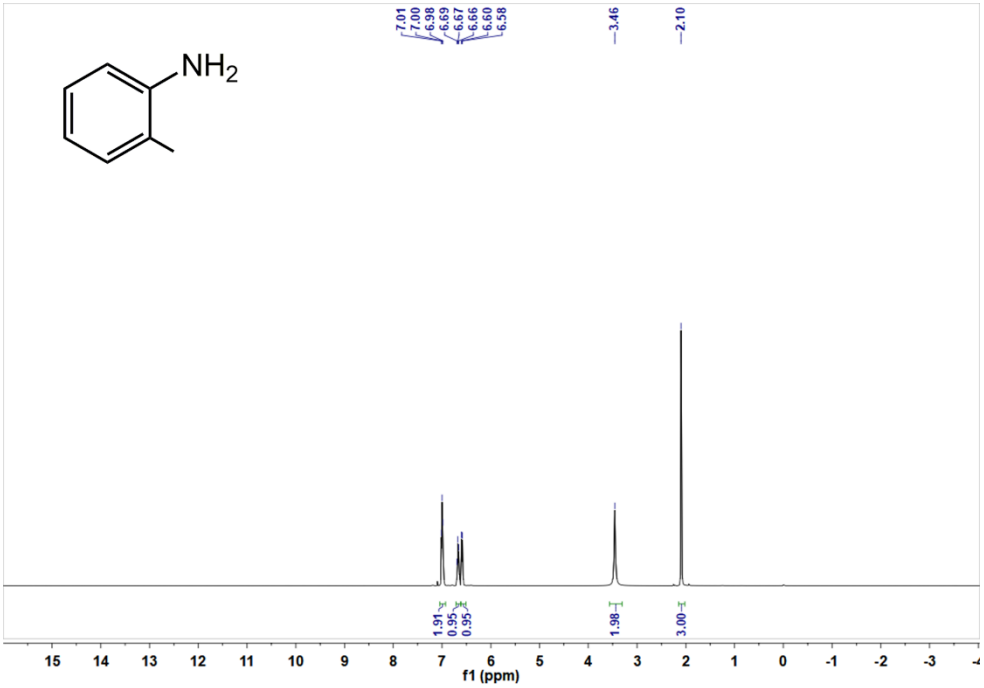

Fig. S24 ^{1}H NMR spectra of **2d** (500 MHz, $CDCl_3$).

o-Toluidine (2d): ^{1}H NMR (500 MHz, $CDCl_3$) δ 7.00 (t, J = 6.0 Hz, 2H), 6.68 (t, J = 6.7 Hz, 1H), 6.59 (d, J = 8.1 Hz, 1H), 3.46 (s, 2H), 2.10 (s, 3H).

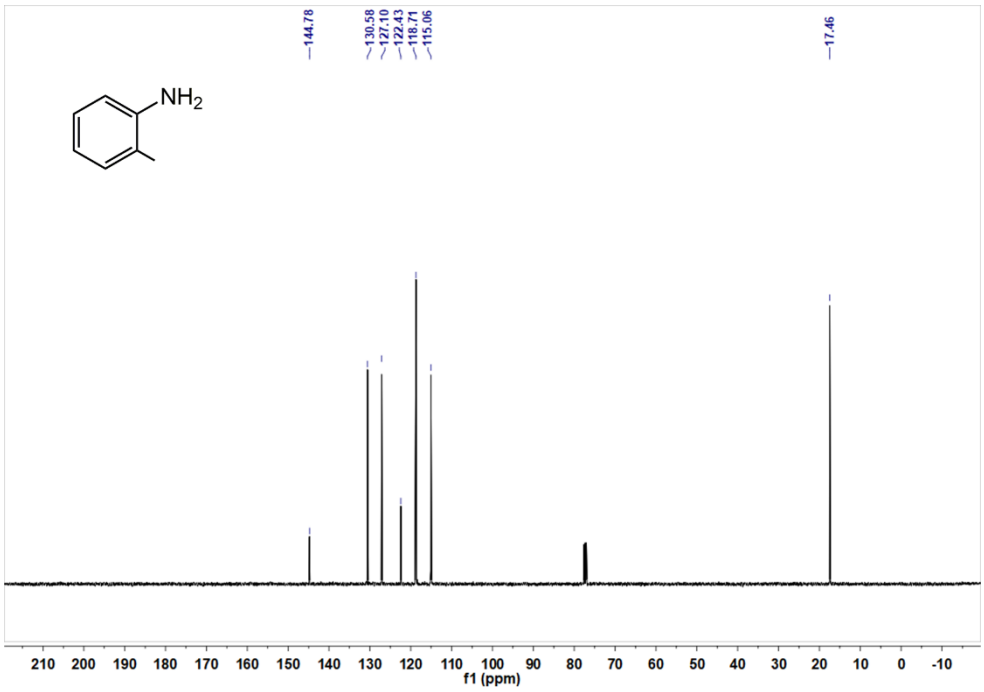

Fig. S25 ^{13}C NMR spectra of **2d** (126 MHz, $CDCl_3$).

o-Toluidine (2d): ^{13}C NMR (126 MHz, $CDCl_3$) δ 144.78 (s), 130.58 (s), 127.10 (s), 122.43 (s), 118.71 (s), 115.06 (s), 17.46 (s).

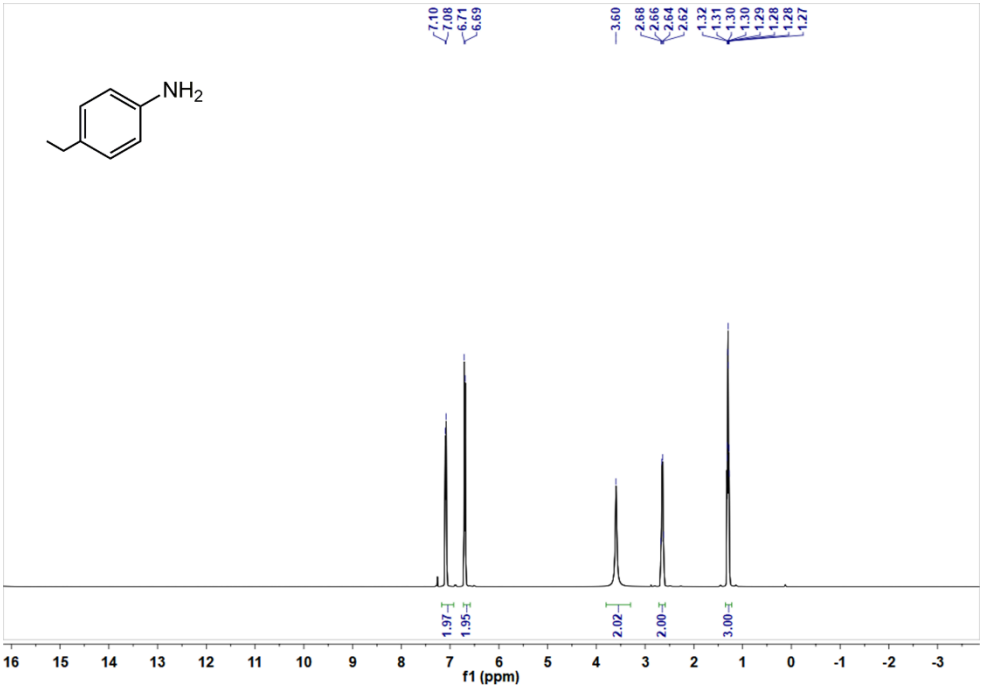

Fig. S26 ^{1}H NMR spectra of **2e** (500 MHz, $CDCl_3$).

4-Ethylaniline (2e): ^{1}H NMR (500 MHz, $CDCl_3$) δ 7.09 (d, J = 8.3 Hz, 2H), 6.70 (d, J = 8.3 Hz, 2H), 3.60 (s, 2H), 2.65 (q, J = 7.5 Hz, 2H), 1.29 (ddd, J = 7.6, 4.9, 2.1 Hz, 3H).

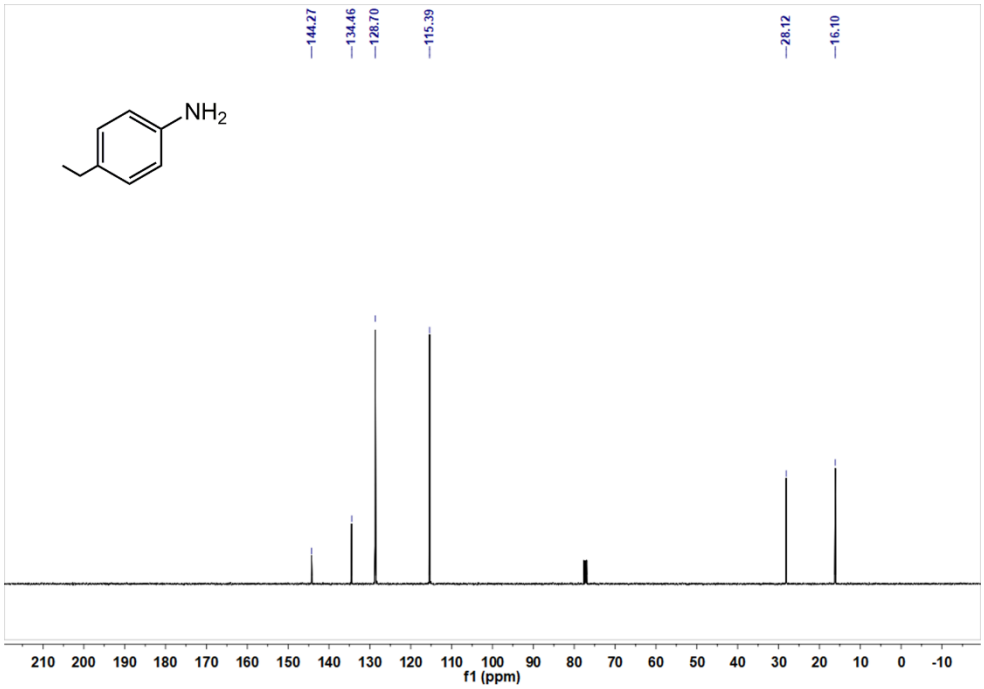

Fig. S27 ^{13}C NMR spectra of **2e** (126 MHz, $CDCl_3$).

4-Ethylaniline (2e): ^{13}C NMR (126 MHz, $CDCl_3$) δ 144.27 (s), 134.46 (s), 128.70 (s), 115.39 (s), 28.12 (s), 16.10 (s).

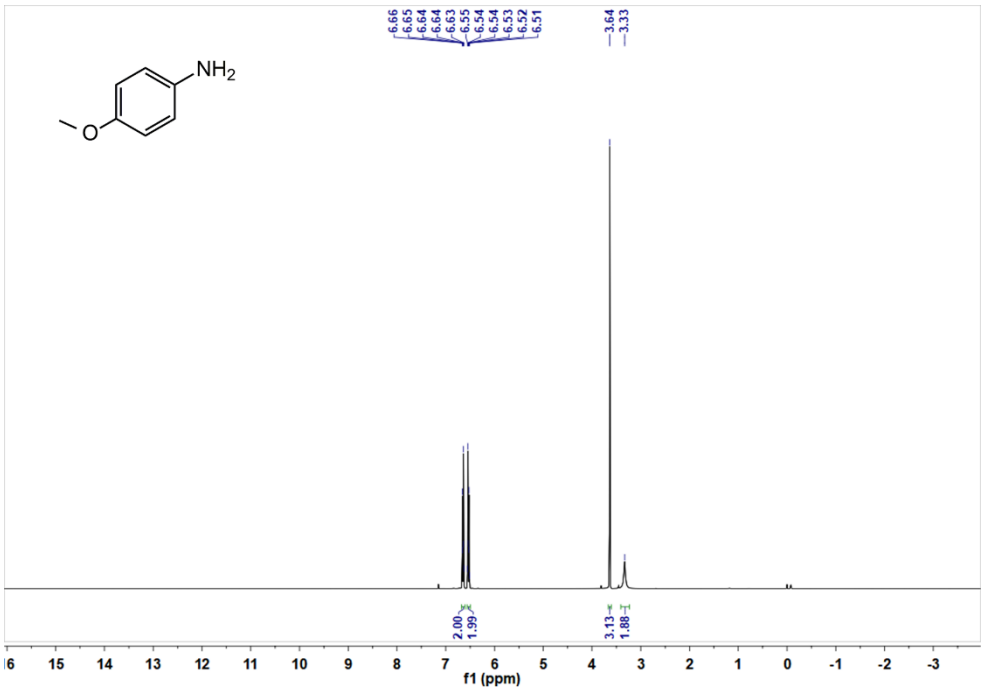

Fig. S28 ^{1}H NMR spectra of **2f** (500 MHz, $CDCl_3$).

p-Anisidine (2f): ^{1}H NMR (500 MHz, $CDCl_3$) δ 6.68 – 6.61 (m, 2H), 6.56 – 6.50 (m, 2H), 3.64 (s, 3H), 3.33 (s, 2H).

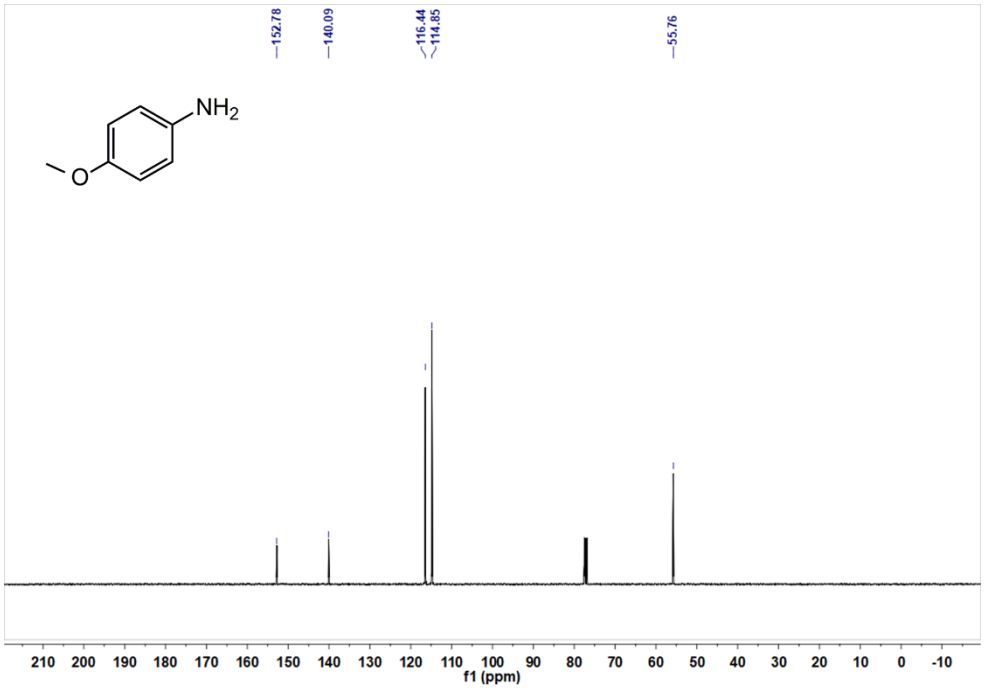

Fig. S29 ^{13}C NMR spectra of **2f** (126 MHz, $CDCl_3$).

p-Anisidine (2f): ^{13}C NMR (126 MHz, $CDCl_3$) δ 152.78 (s), 140.09 (s), 116.44 (s), 114.85 (s), 55.76 (s).

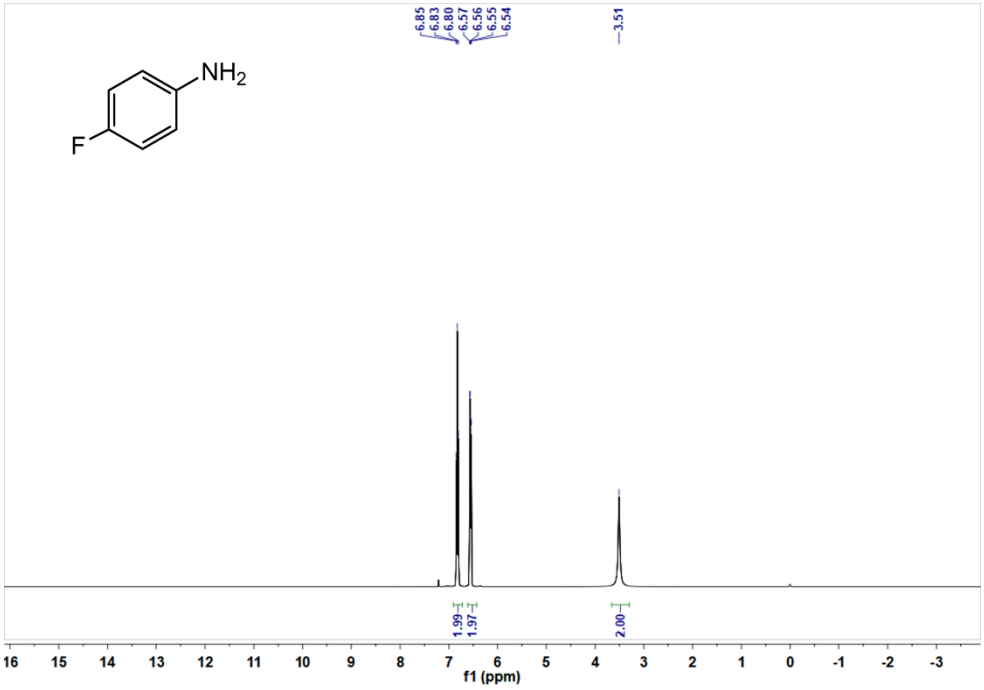

Fig. S30 ^{1}H NMR spectra of **2g** (500 MHz, $CDCl_3$).

4-Fluoroaniline (2g): ^{1}H NMR (500 MHz, $CDCl_3$) δ 6.83 (t, J = 8.7 Hz, 2H), 6.56 (dd, J = 8.9, 4.5 Hz, 2H), 3.51 (s, 2H).

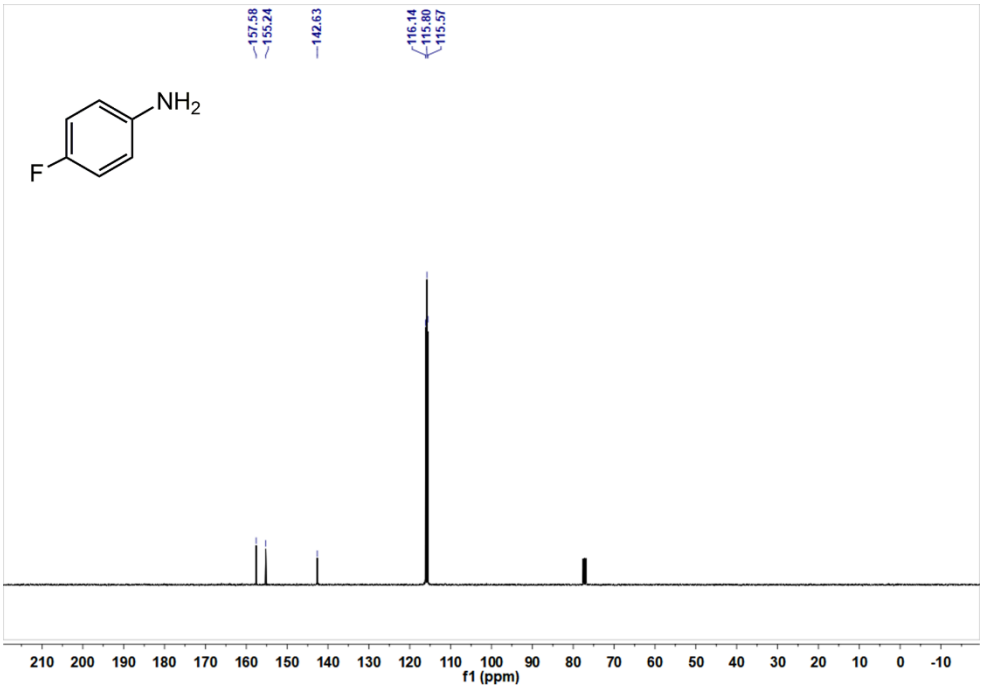

Fig. S31 ^{13}C NMR spectra of **2g** (126 MHz, $CDCl_3$).

4-Fluoroaniline (2g):^{13}C NMR (126 MHz, $CDCl_3$) δ 157.58 (s), 155.24 (s), 142.63 (s), 116.14 (s), 115.80 (s), 115.57 (s).

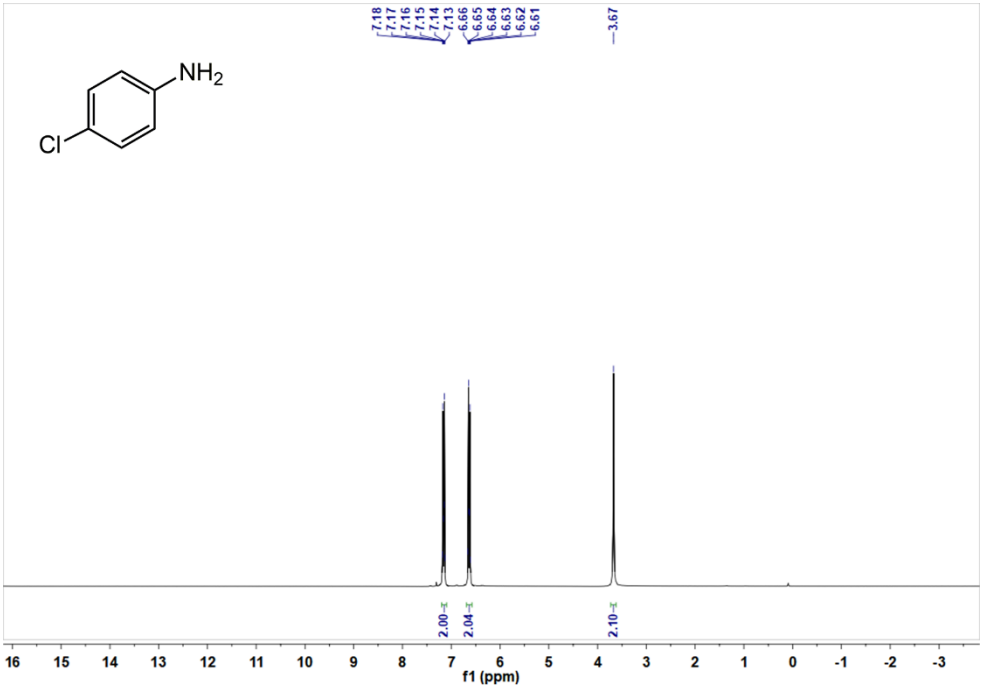

Fig. S32 ^{1}H NMR spectra of **2h** (500 MHz, $CDCl_3$).

4-Chloroaniline (2h): ^{1}H NMR (500 MHz, $CDCl_3$) δ 7.20 – 7.10 (m, 2H), 6.69 – 6.58 (m, 2H), 3.67 (s, 2H).

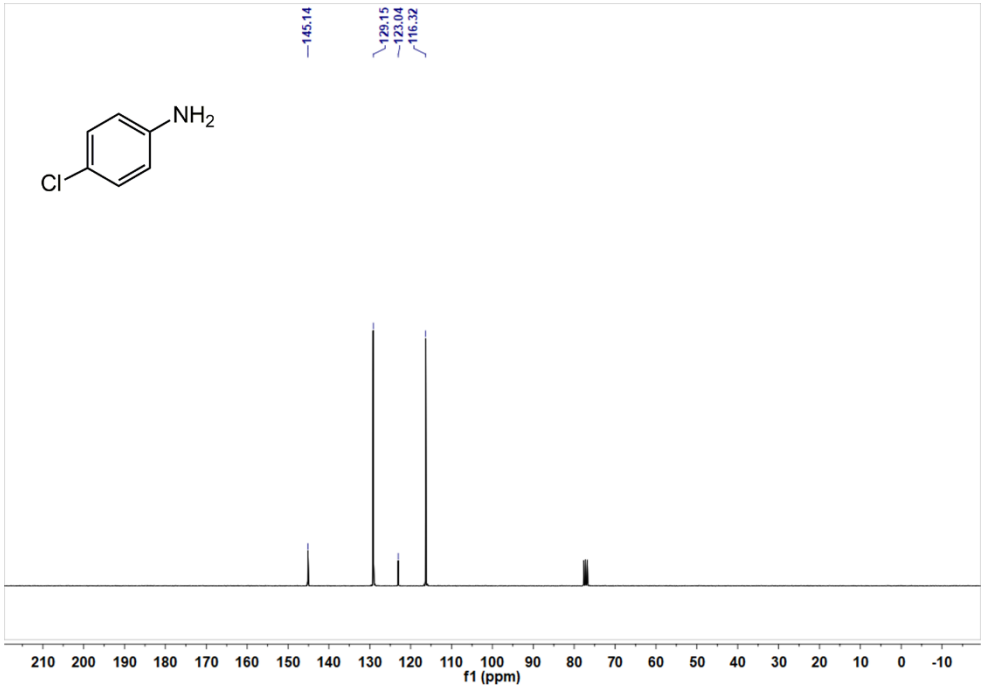

Fig. S33 ^{13}C NMR spectra of **2h** (126 MHz, $CDCl_3$).

4-Chloroaniline (2h): ^{13}C NMR (126 MHz, $CDCl_3$) δ 145.14 (s), 129.15 (s), 123.04 (s), 116.32 (s).

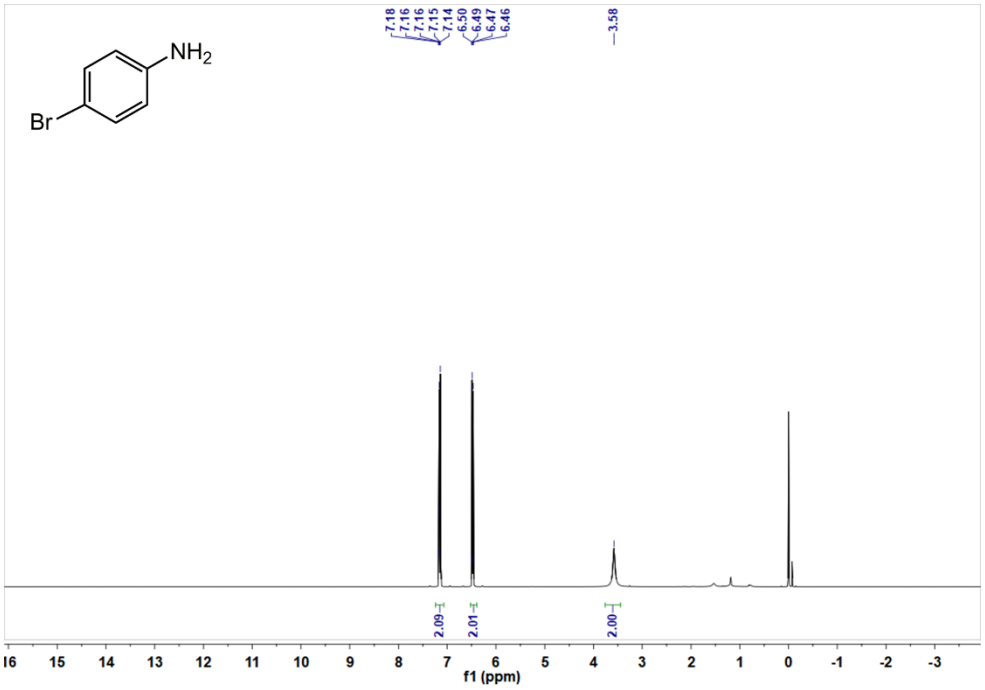

Fig. S34 ^{1}H NMR spectra of **2i** (500 MHz, $CDCl_3$).

4-Bromoaniline (2i): ^{1}H NMR (500 MHz, $CDCl_3$) δ 7.24 – 7.07 (m, 2H), 6.52 – 6.40 (m, 2H), 3.58 (s, 2H).

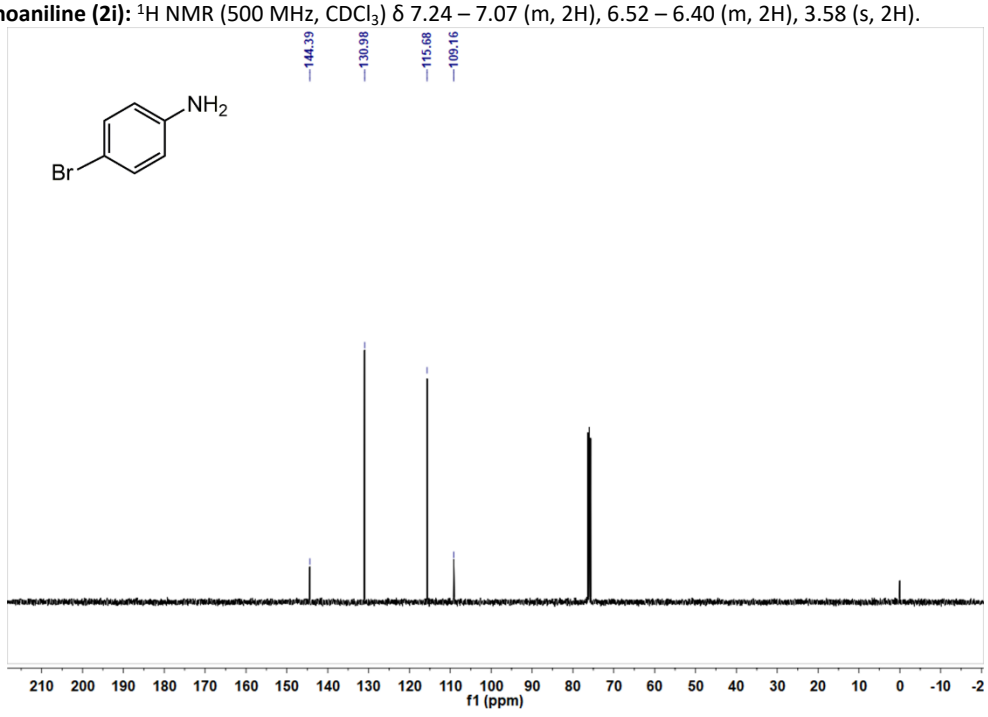

Fig. S35 ^{13}C NMR spectra of **2i** (126 MHz, $CDCl_3$).

4-Bromoaniline (2i): ^{13}C NMR (126 MHz, $CDCl_3$) δ 144.39 (s), 130.98 (s), 115.68 (s), 109.16 (s).

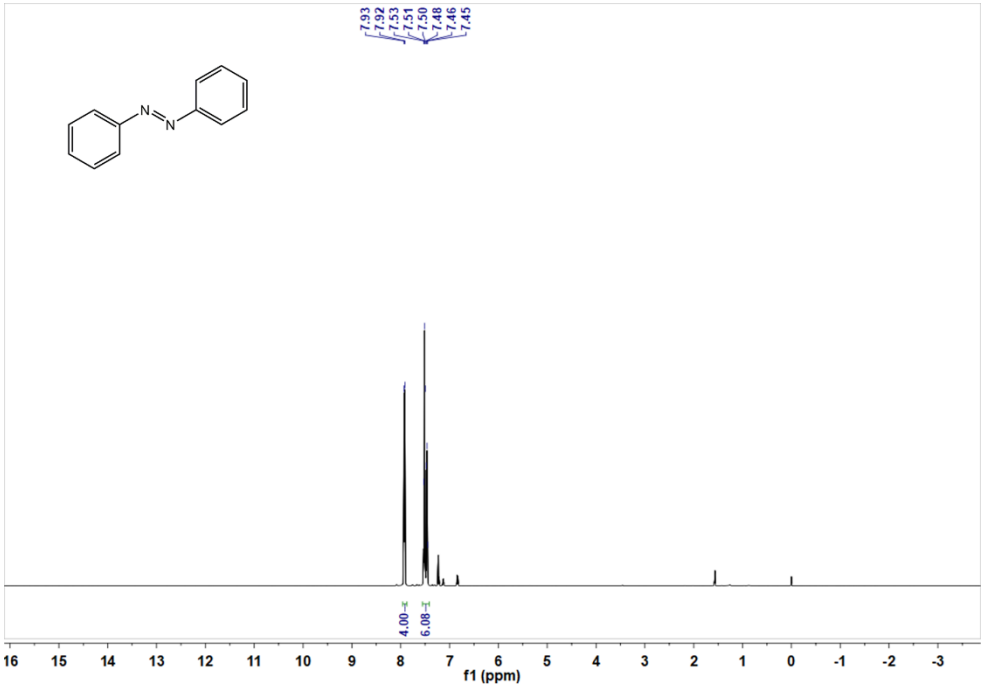

Fig. S36 ^{1}H NMR spectra of **3a** (500 MHz, $CDCl_3$).

Azobenzene (3a): ^{1}H NMR (500 MHz, $CDCl_3$) δ 7.92 (d, J = 8.2 Hz, 4H), 7.49 (dt, J = 24.3, 7.1 Hz, 6H).

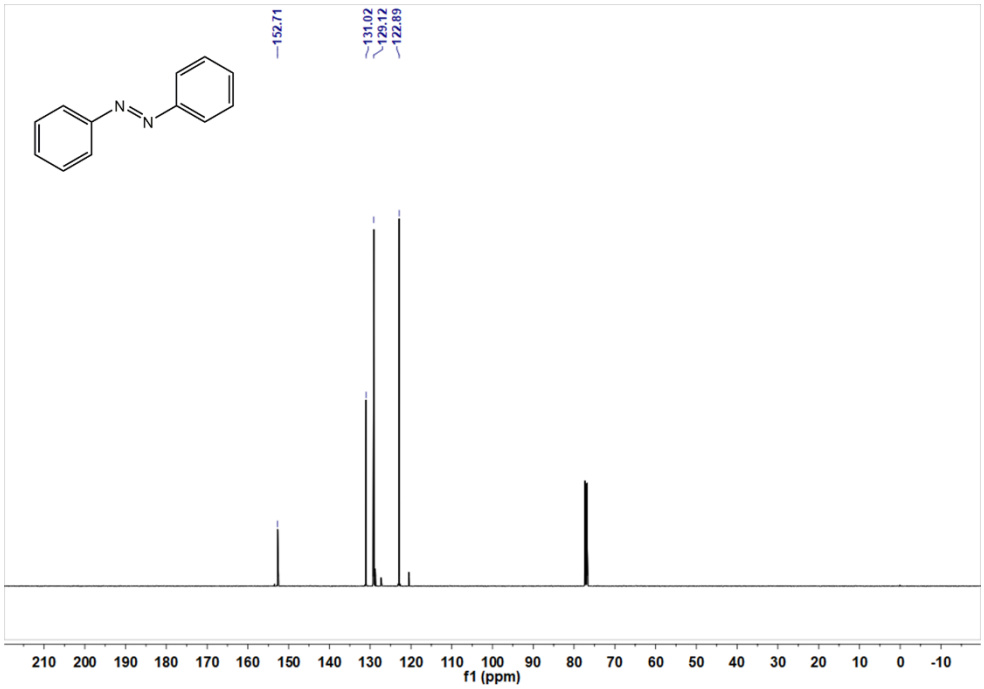

Fig. S37 ^{13}C NMR spectra of **3a** (126 MHz, $CDCl_3$).

Azobenzene (3a): ^{13}C NMR (126 MHz, $CDCl_3$) δ 152.71 (s), 131.02 (s), 129.12 (s), 122.89 (s).

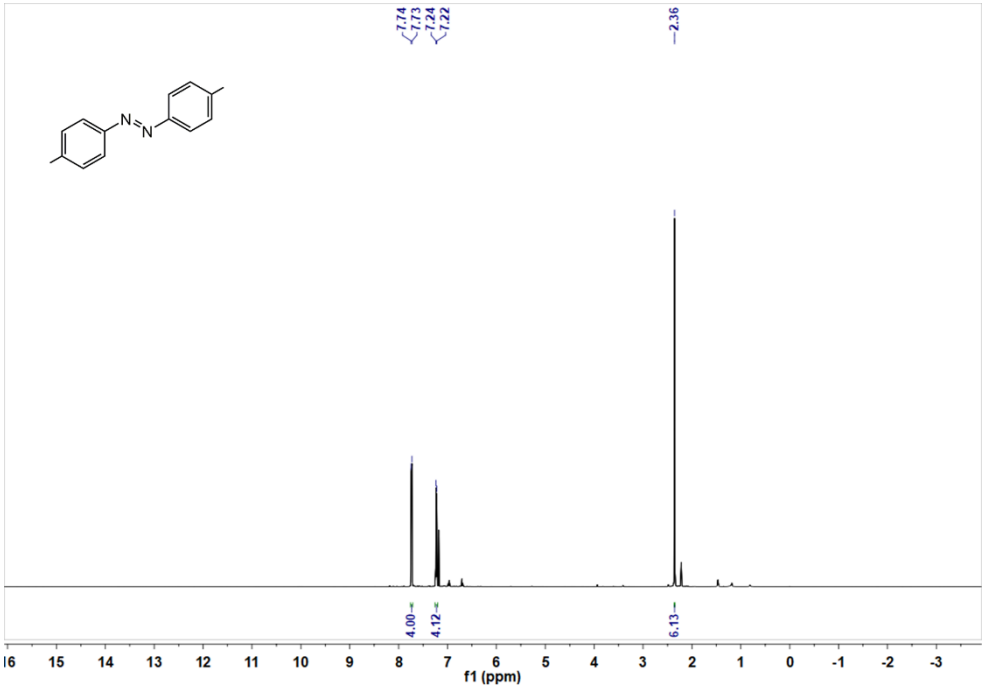

Fig. S38 ^{1}H NMR spectra of **3b** (500 MHz, $CDCl_3$).

(E)-1,2-di-p-tolyldiazene (3b): ^{1}H NMR (500 MHz, $CDCl_3$) δ 7.74 (d, J = 8.3 Hz, 4H), 7.23 (d, J = 8.1 Hz, 4H), 2.36 (s, 6H).

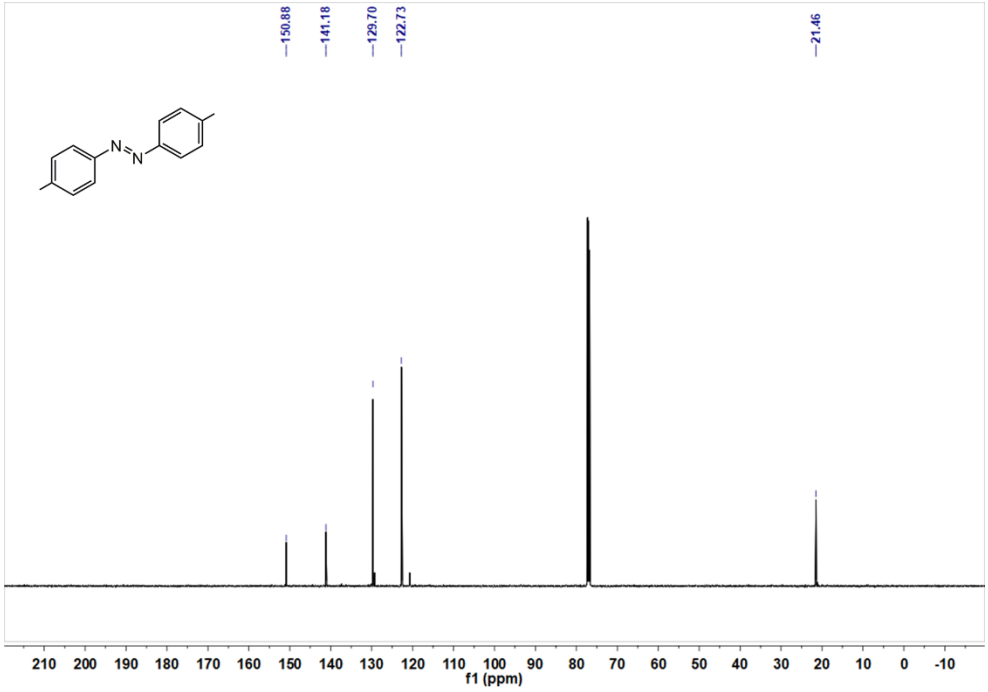

Fig. S39 ^{13}C NMR spectra of **3b** (126 MHz, $CDCl_3$).

(E)-1,2-di-p-tolyldiazene (3b): ^{13}C NMR (126 MHz, $CDCl_3$) δ 150.88 (s), 141.18 (s), 129.70 (s), 122.73 (s), 21.46 (s).

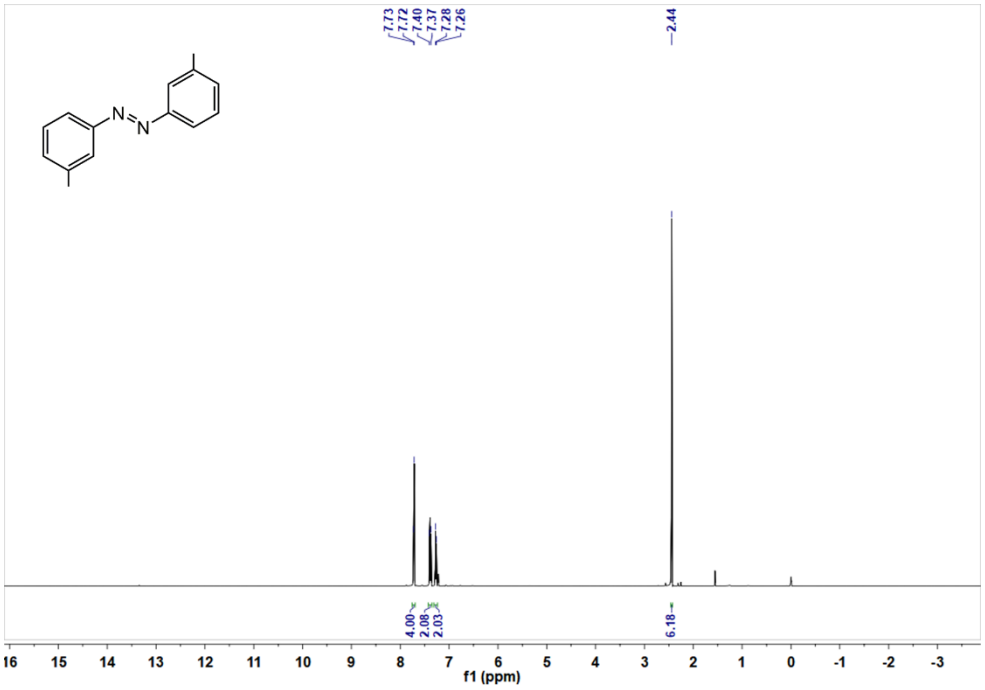

Fig. S40 ^{1}H NMR spectra of **3c** (500 MHz, $CDCl_3$).

(E)-1,2-di-m-tolyldiazene (3c): ^{1}H NMR (500 MHz, $CDCl_3$) δ 7.72 (d, J = 5.9 Hz, 4H), 7.39 (d, J = 16.0 Hz, 2H), 7.27 (d, J = 7.4 Hz, 2H), 2.44 (s, 6H).

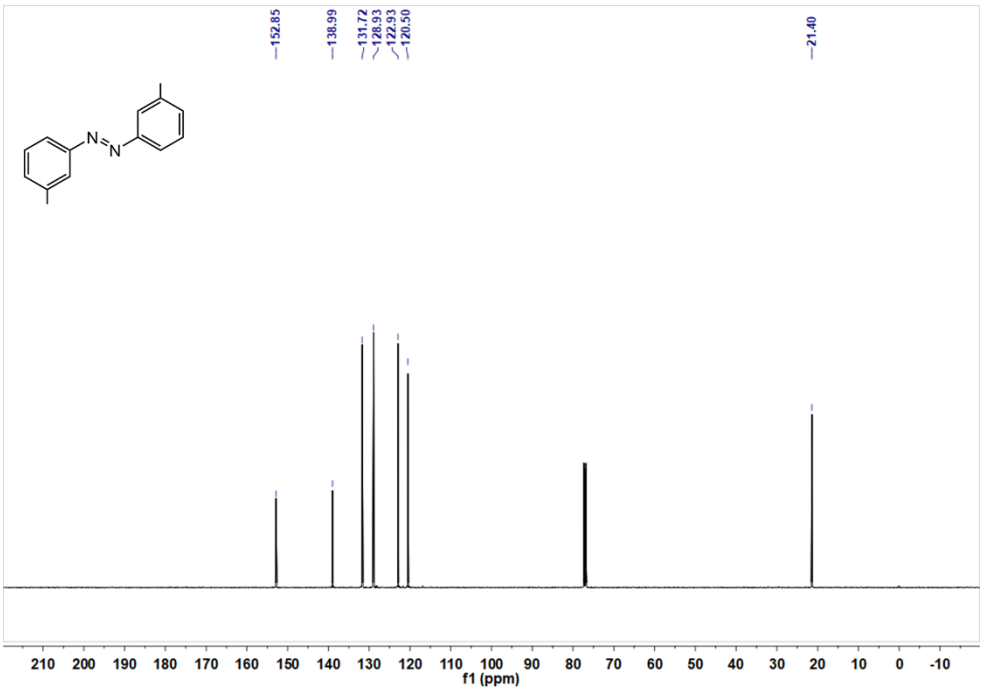

Fig. S41 ^{13}C NMR spectra of **3c** (126 MHz, $CDCl_3$).

(E)-1,2-di-m-tolyldiazene (3c): ^{13}C NMR (126 MHz, $CDCl_3$) δ 152.85 (s), 138.99 (s), 131.72 (s), 128.93 (s), 122.93 (s), 120.50 (s), 21.40 (s).

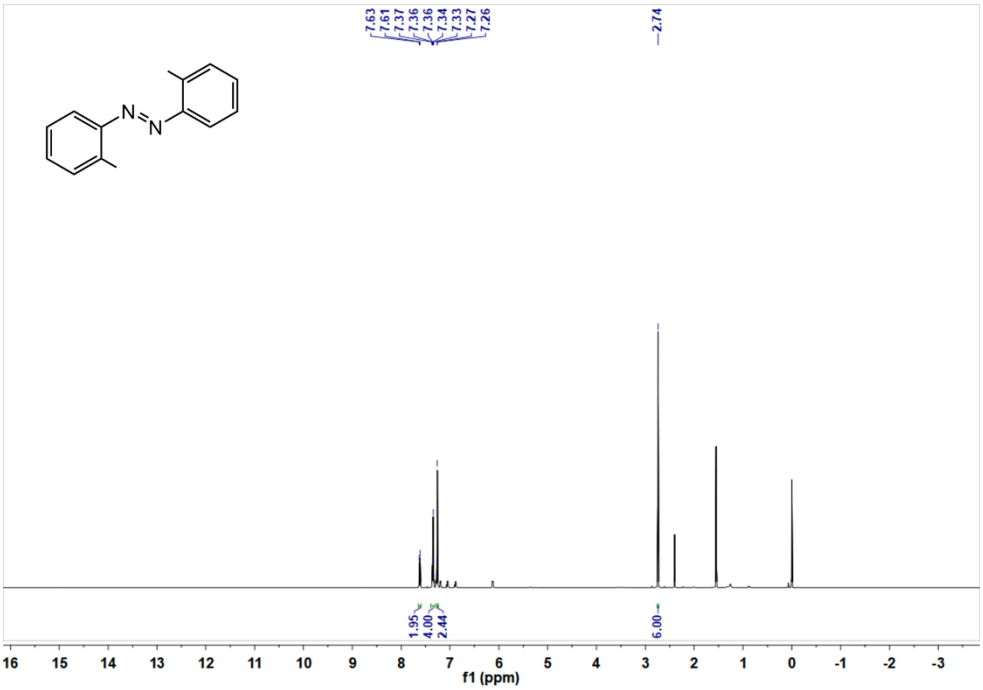

Fig. S42 ^{1}H NMR spectra of **3d** (500 MHz, $CDCl_3$).

(E)-1,2-Di-o-tolyldiazene (3d): ^{1}H NMR (500 MHz, $CDCl_3$) δ 7.62 (d, J = 7.9 Hz, 2H), 7.39 – 7.30 (m, 4H), 7.26 (s, 2H), 2.74 (s, 6H).

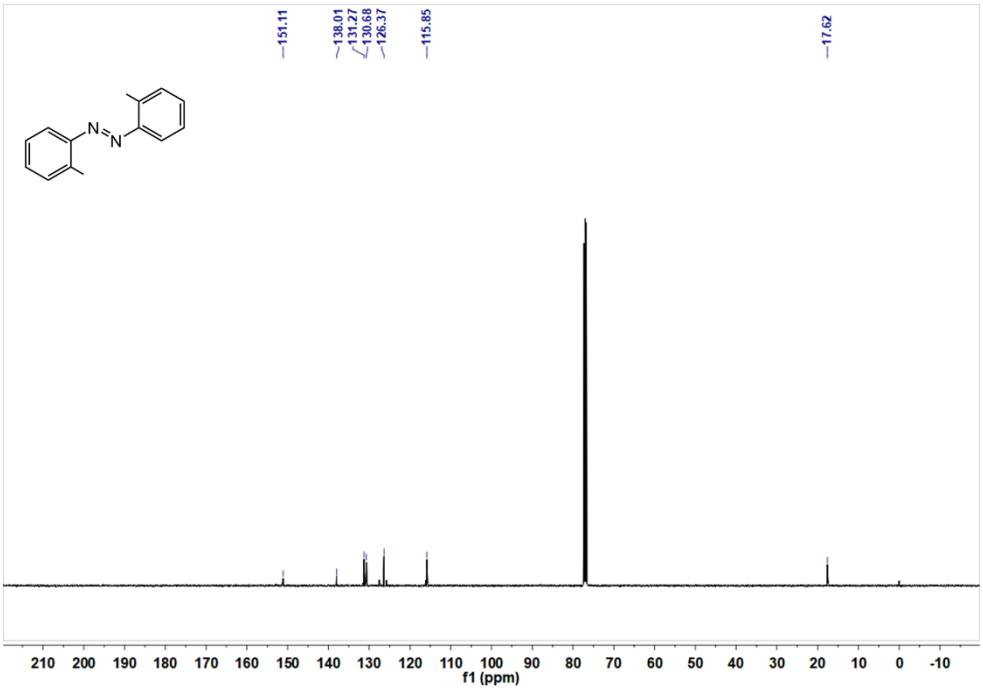

Fig. S43 ^{13}C NMR spectra of **3d** (126 MHz, $CDCl_3$).

(E)-1,2-Di-o-tolyldiazene (3d): ^{13}C NMR (126 MHz, $CDCl_3$) δ 151.11 (s), 138.01 (s), 131.27 (s), 130.68 (s), 126.37 (s), 115.85 (s), 17.62 (s).

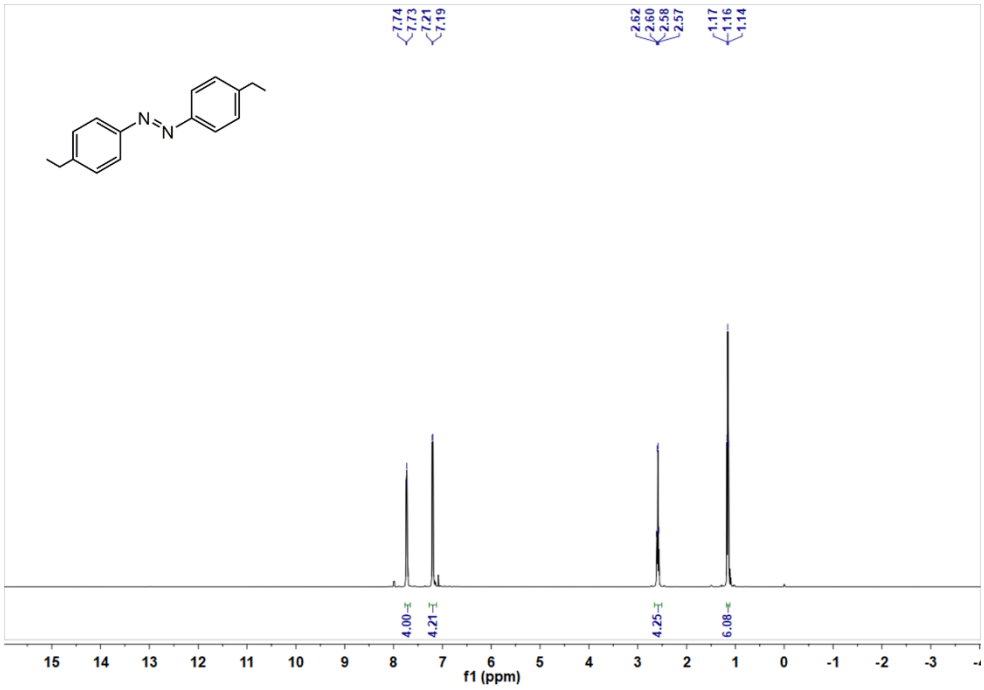

Fig. S44 ^{1}H NMR spectra of **3e** (500 MHz, $CDCl_3$).

(E)-1,2-bis(4-ethylphenyl)diazene (3e): ^{1}H NMR (500 MHz, $CDCl_3$) δ 7.74 (d, J = 8.2 Hz, 4H), 7.20 (d, J = 8.1 Hz, 4H), 2.59 (q, J = 7.6 Hz, 4H), 1.16 (t, J = 7.6 Hz, 6H).

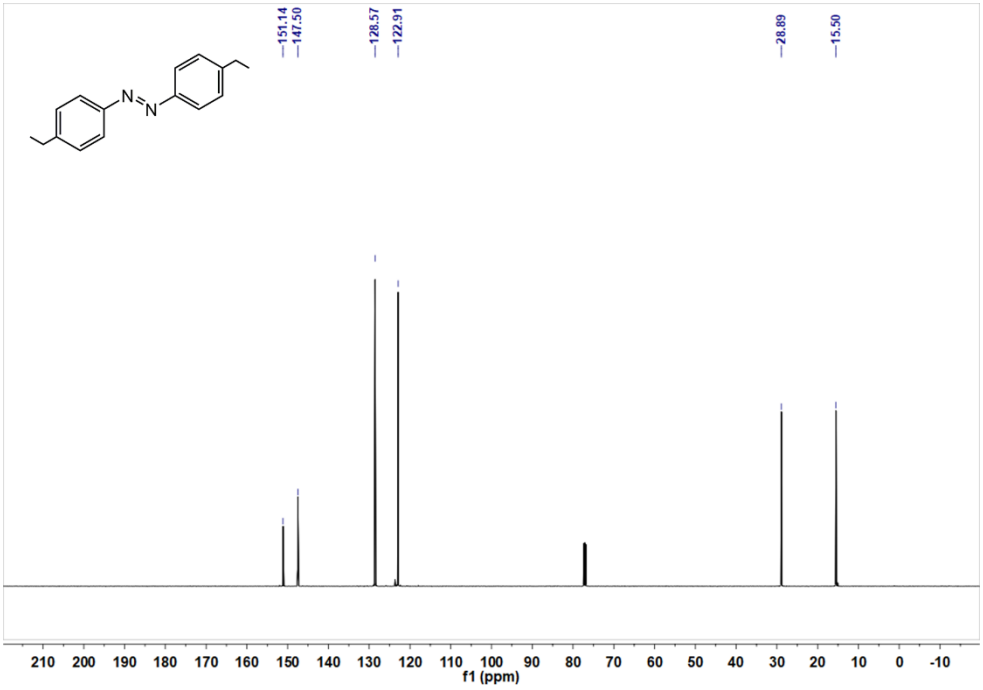

Fig. S45 ^{13}C NMR spectra of **3e** (126 MHz, $CDCl_3$).

(E)-1,2-bis(4-ethylphenyl)diazene (3e): ^{13}C NMR (126 MHz, $CDCl_3$) δ 151.14 (s), 147.50 (s), 128.57 (s), 122.91 (s), 28.89 (s), 15.50 (s).

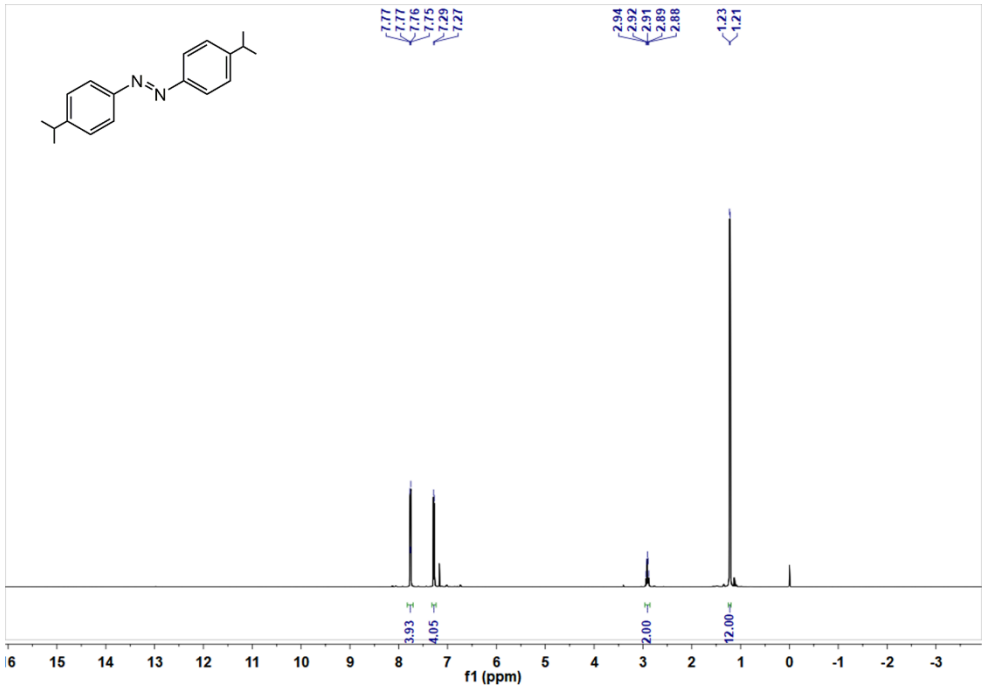

Fig. S46 ^{1}H NMR spectra of **3f** (500 MHz, $CDCl_3$).

(E)-1,2-bis(4-isopropylphenyl)diazene (3f): ^{1}H NMR (500 MHz, $CDCl_3$) δ 7.83 – 7.70 (m, 4H), 7.28 (d, J = 8.3 Hz, 4H), 2.91 (dt, J = 13.8, 6.9 Hz, 2H), 1.22 (d, J = 6.9 Hz, 12H).

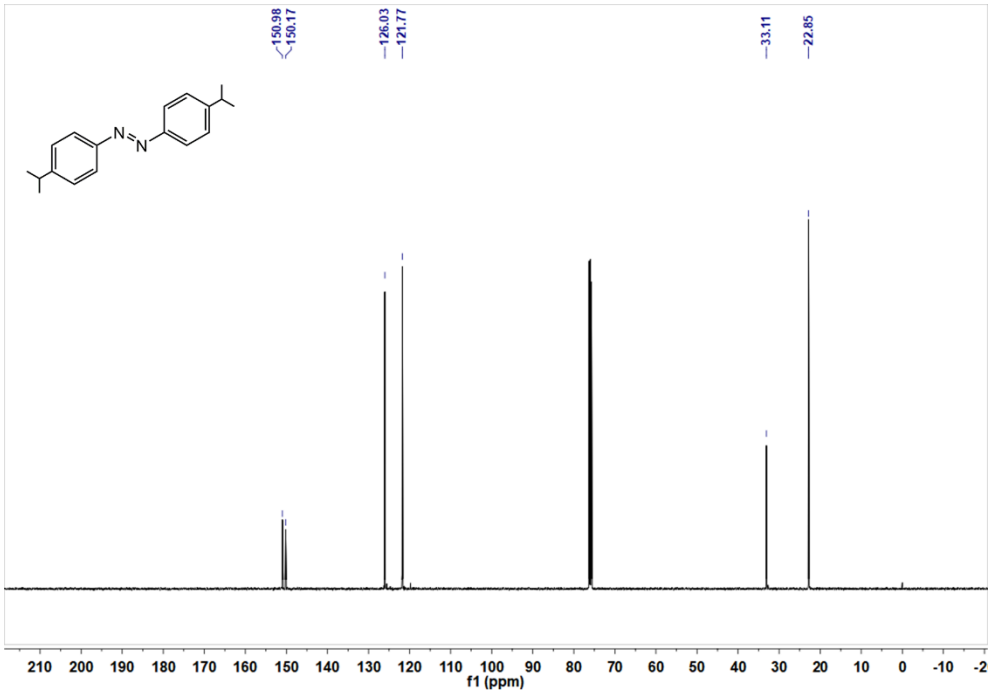

Fig. S47 ^{13}C NMR spectra of **3f** (126 MHz, $CDCl_3$).

(E)-1,2-bis(4-isopropylphenyl)diazene (3f): ^{13}C NMR (126 MHz, $CDCl_3$) δ 150.98 (s), 150.17 (s), 126.03 (s), 121.77 (s), 33.11 (s), 22.85 (s).

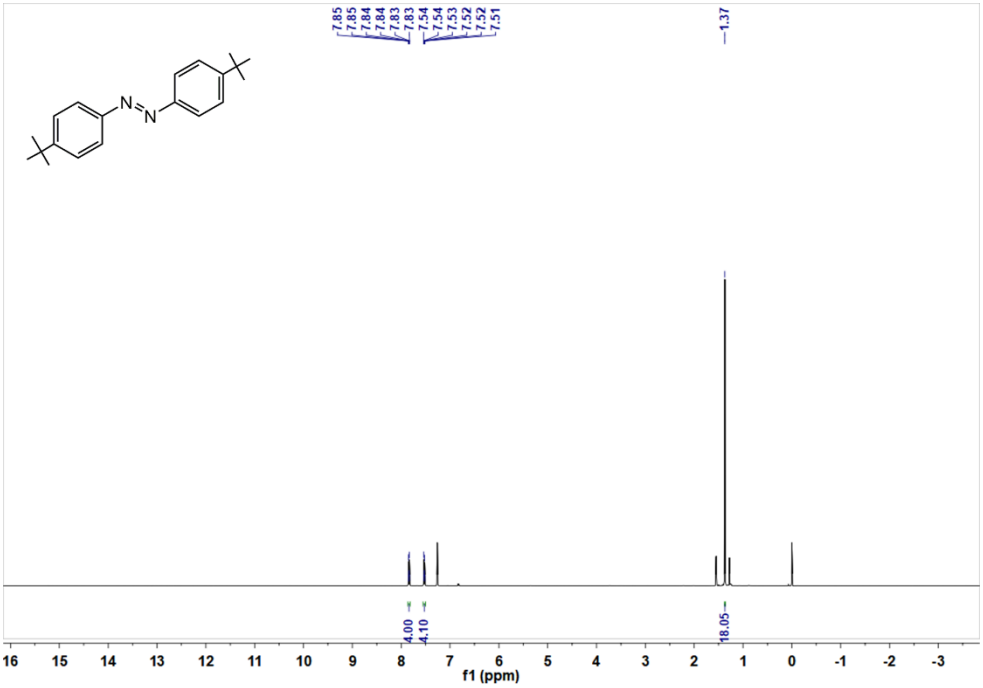

Fig. S48 ^{1}H NMR spectra of **3g** (500 MHz, $CDCl_3$).

(E)-1,2-bis(4-tert-butyl-phenyl)-diazene (3g): ^{1}H NMR (500 MHz, $CDCl_3$) δ 7.86 – 7.82 (m, 4H), 7.55 – 7.50 (m, 4H), 1.37 (s, 18H).

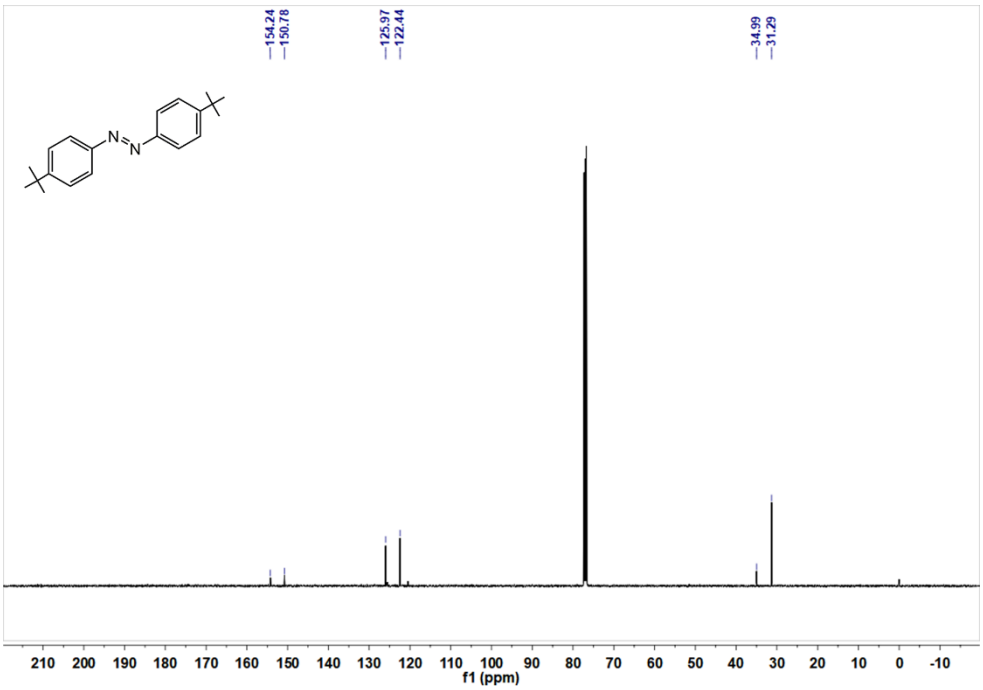

Fig. S49 ^{13}C NMR spectra of **3g** (126 MHz, $CDCl_3$).

(E)-1,2-bis(4-tert-butyl-phenyl)-diazene (3g): ^{13}C NMR (126 MHz, $CDCl_3$) δ 154.24 (s), 150.78 (s), 125.97 (s), 122.44 (s), 34.99 (s), 31.29 (s).

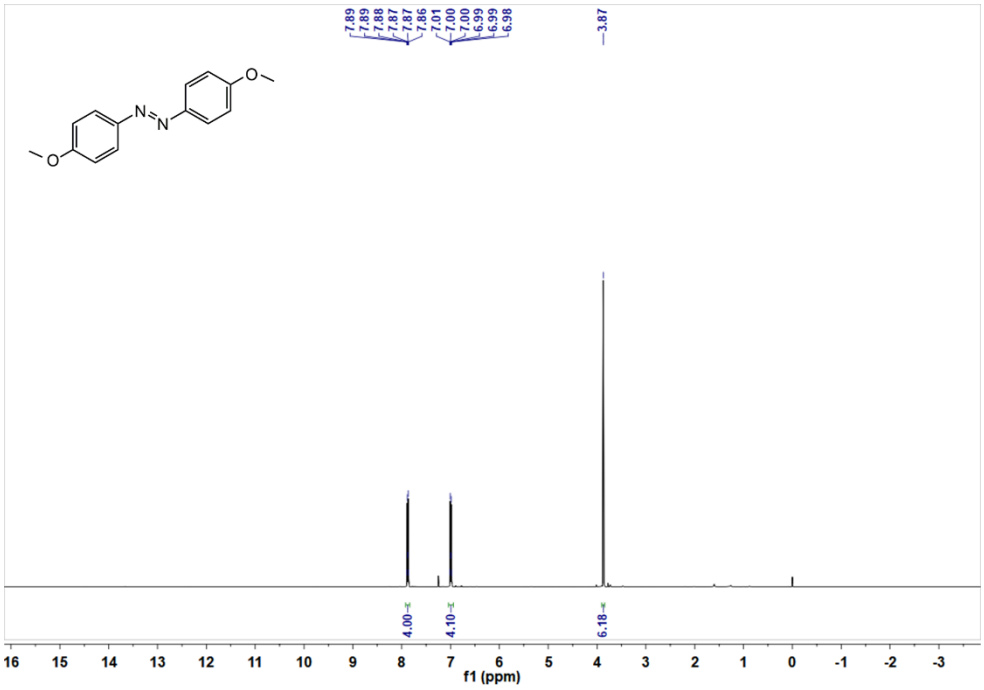

Fig. S50 ^{1}H NMR spectra of **3h** (500 MHz, $CDCl_3$).

(E)-1,2-Bis(4-methoxyphenyl)diazene (3h): ^{1}H NMR (500 MHz, $CDCl_3$) δ 7.92 – 7.83 (m, 4H), 7.04 – 6.94 (m, 4H), 3.87 (s, 6H).

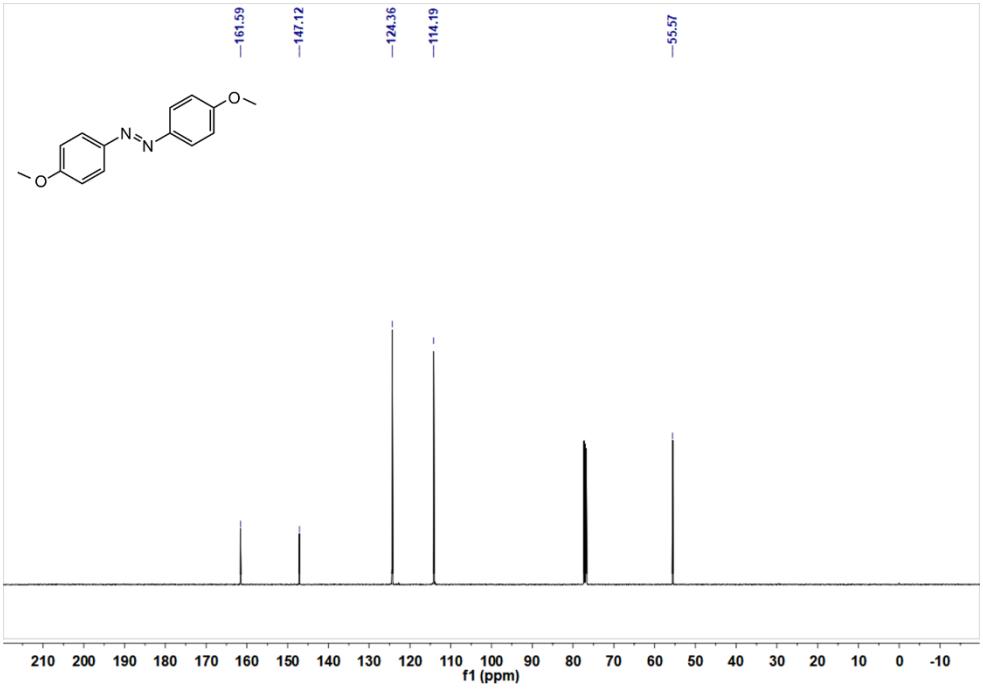

Fig. S51 ^{13}C NMR spectra of **3h** (126 MHz, $CDCl_3$).

(E)-1,2-Bis(4-methoxyphenyl)diazene (3h): ^{13}C NMR (126 MHz, $CDCl_3$) δ 161.59 (s), 147.12 (s), 124.36 (s), 114.19 (s), 55.57 (s).

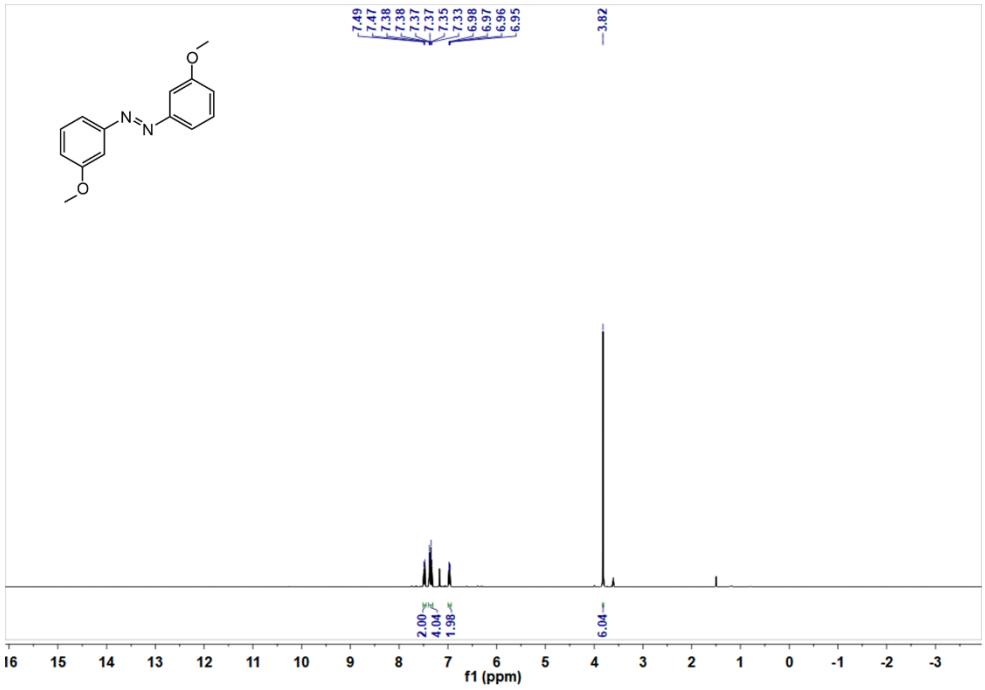

Fig. S52 ^{1}H NMR spectra of **3i** (500 MHz, $CDCl_3$).

(E)-1,2-bis(3-methoxyphenyl)diazene (3i): ^{1}H NMR (500 MHz, $CDCl_3$) δ 7.48 (d, J = 8.6 Hz, 2H), 7.36 (dt, J = 16.1, 5.1 Hz, 4H), 6.97 (dd, J = 8.2, 2.6 Hz, 2H), 3.82 (s, 6H).

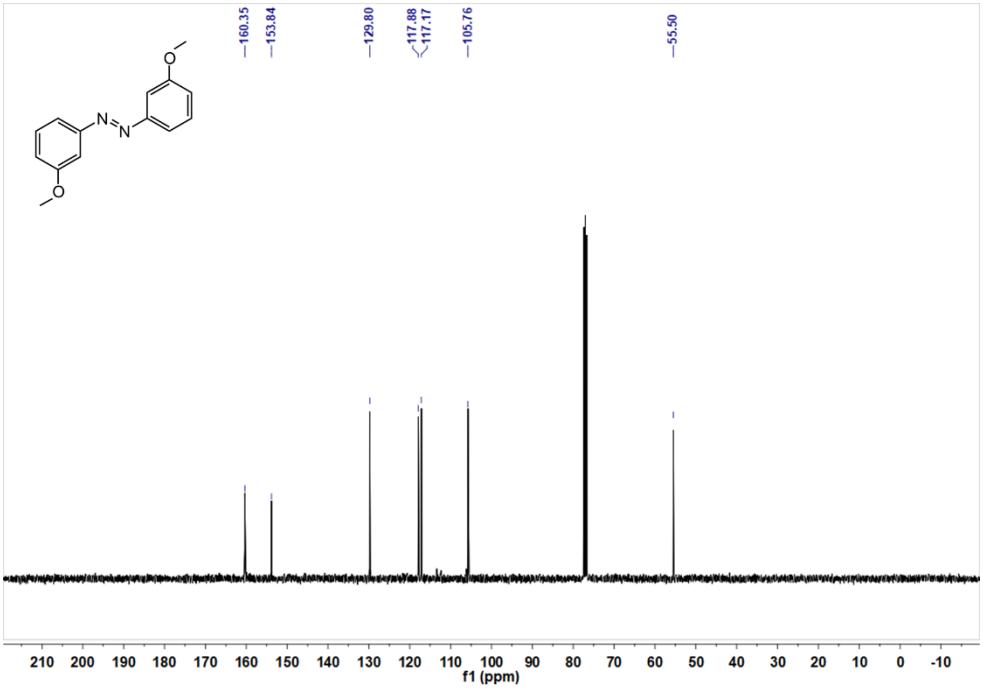

Fig. S53 ^{13}C NMR spectra of **3i** (126 MHz, $CDCl_3$).

(E)-1,2-bis(3-methoxyphenyl)diazene (3i): ^{13}C NMR (126 MHz, $CDCl_3$) δ 160.35 (s), 153.84 (s), 129.80 (s), 117.88 (s), 117.17 (s), 105.76 (s), 55.50 (s).

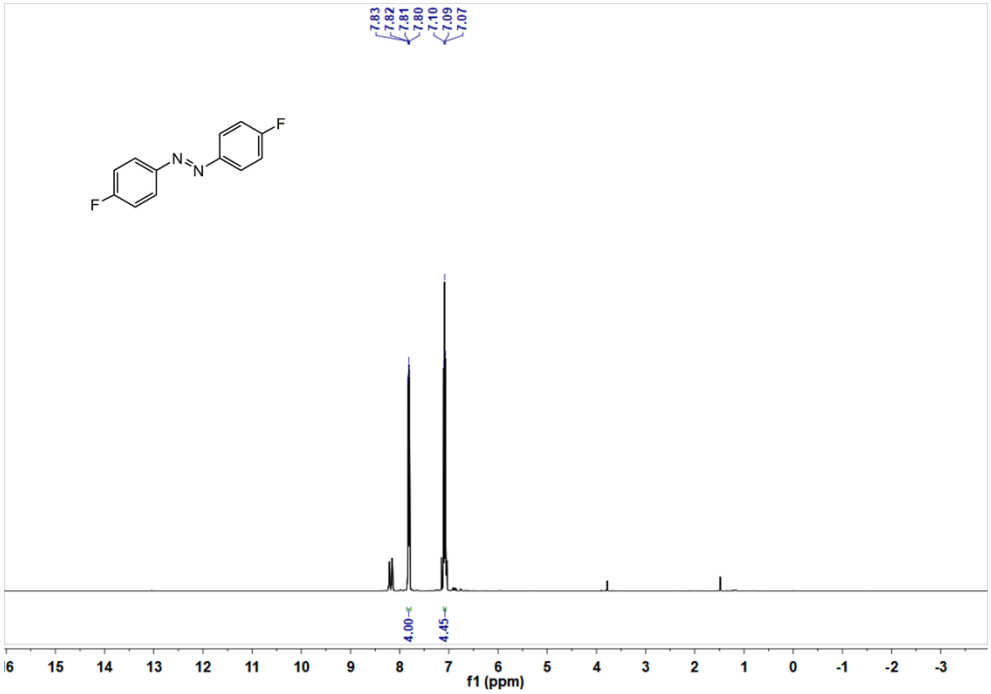

Fig. S54 ^{1}H NMR spectra of **3j** (500 MHz, $CDCl_3$).

(E)-1,2-bis(4-fluorophenyl)diazene (3j): ^{1}H NMR (500 MHz, $CDCl_3$) δ 7.82 (dd, J = 9.0, 5.2 Hz, 4H), 7.11 – 7.06 (m, 4H).

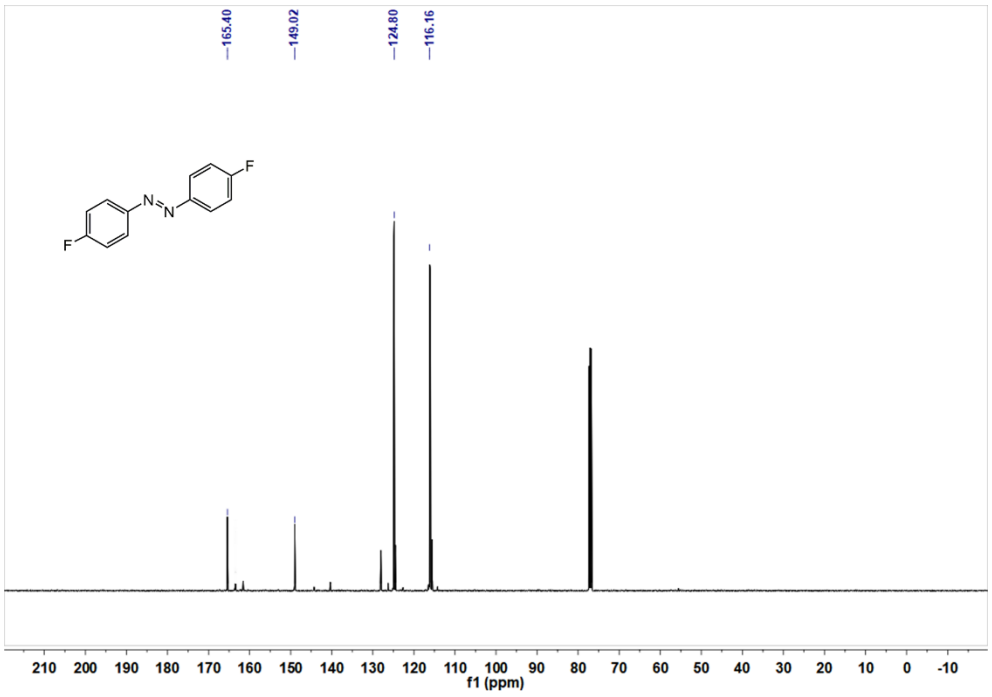

Fig. S55 ^{13}C NMR spectra of **3j** (126 MHz, $CDCl_3$).

€-1,2-bis(4-fluorophenyl)diazene (3j): ^{13}C NMR (126 MHz, $CDCl_3$) δ 165.40 (s), 149.02 (s), 124.80 (s), 116.16 (s).

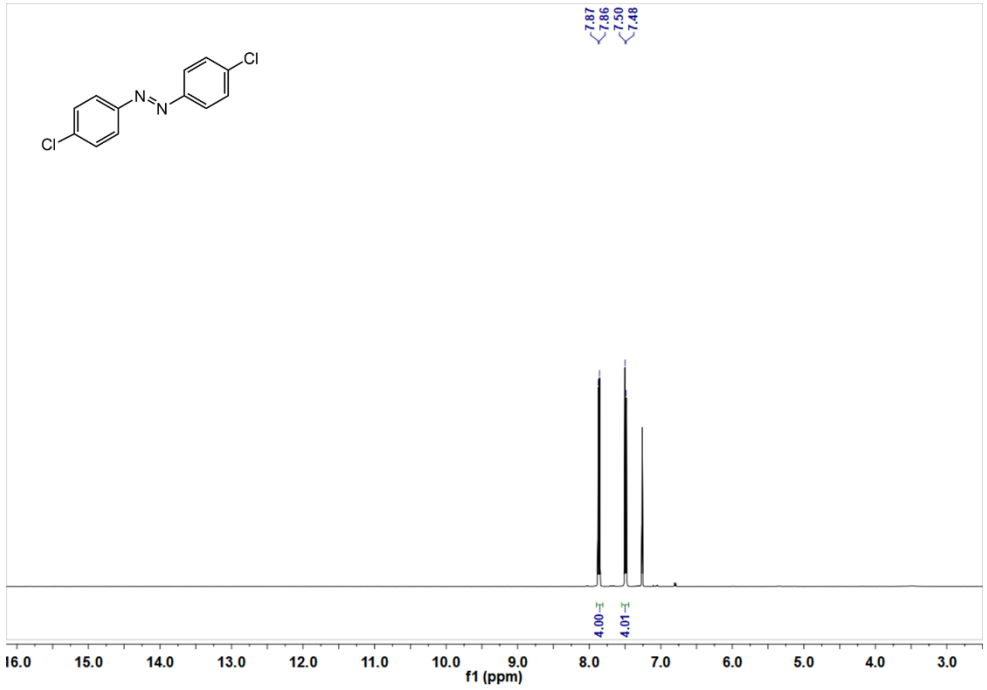

Fig. S56 ^{1}H NMR spectra of **3k** (500 MHz, $CDCl_3$).

(E)-1,2-bis(4-chlorophenyl)diazene (3k): ^{1}H NMR (500 MHz, $CDCl_3$) δ 7.87 (d, J = 8.7 Hz, 4H), 7.49 (d, J = 8.7 Hz, 4H).

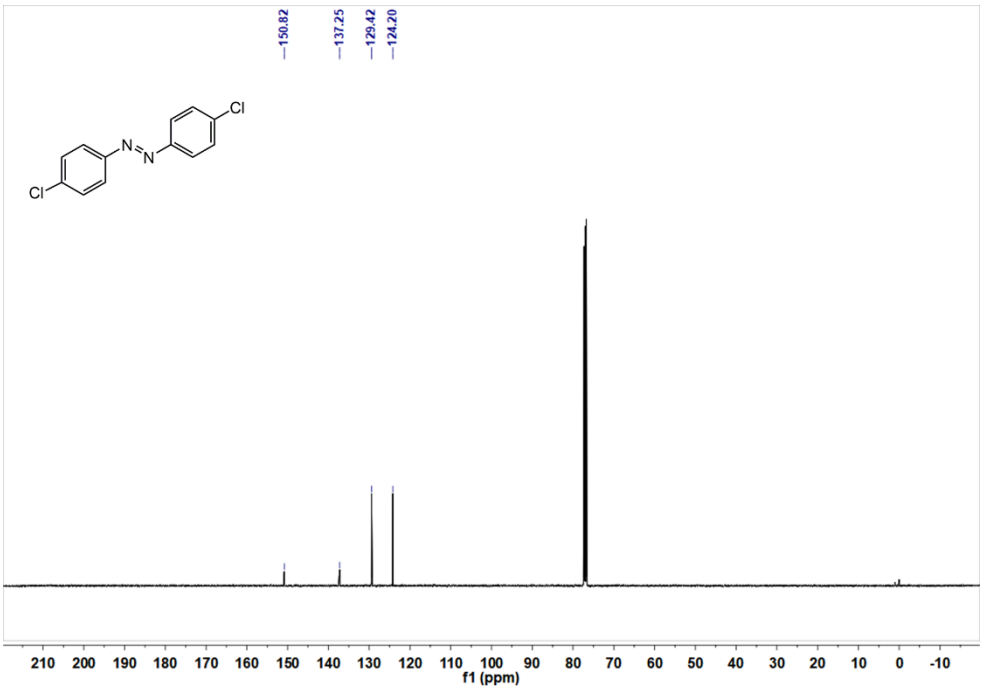

Fig. S57 ^{13}C NMR spectra of **3k** (126 MHz, $CDCl_3$).

(E)-1,2-bis(4-chlorophenyl)diazene (3k): ^{13}C NMR (126 MHz, $CDCl_3$) δ 150.82 (s), 137.25 (s), 129.42 (s), 124.20 (s).

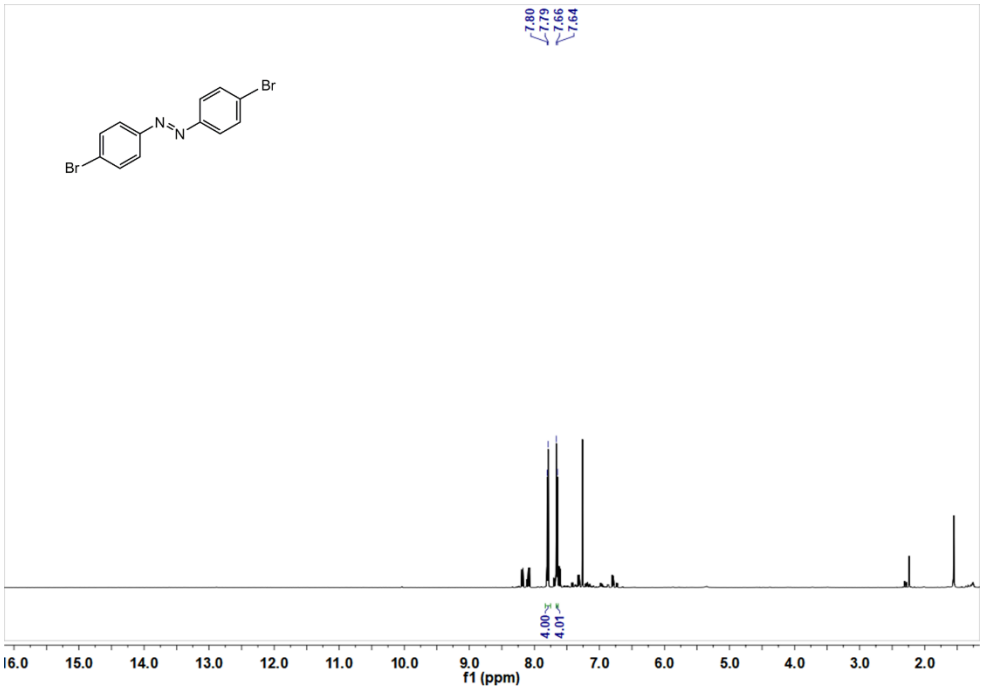

Fig. S58 ^{1}H NMR spectra of **3l** (500 MHz, $CDCl_3$).

(E)-1,2-bis(4-bromophenyl)diazene (3l): ^{1}H NMR (500 MHz, $CDCl_3$) δ 7.80 (d, J = 8.7 Hz, 4H), 7.65 (d, J = 8.8 Hz, 4H).

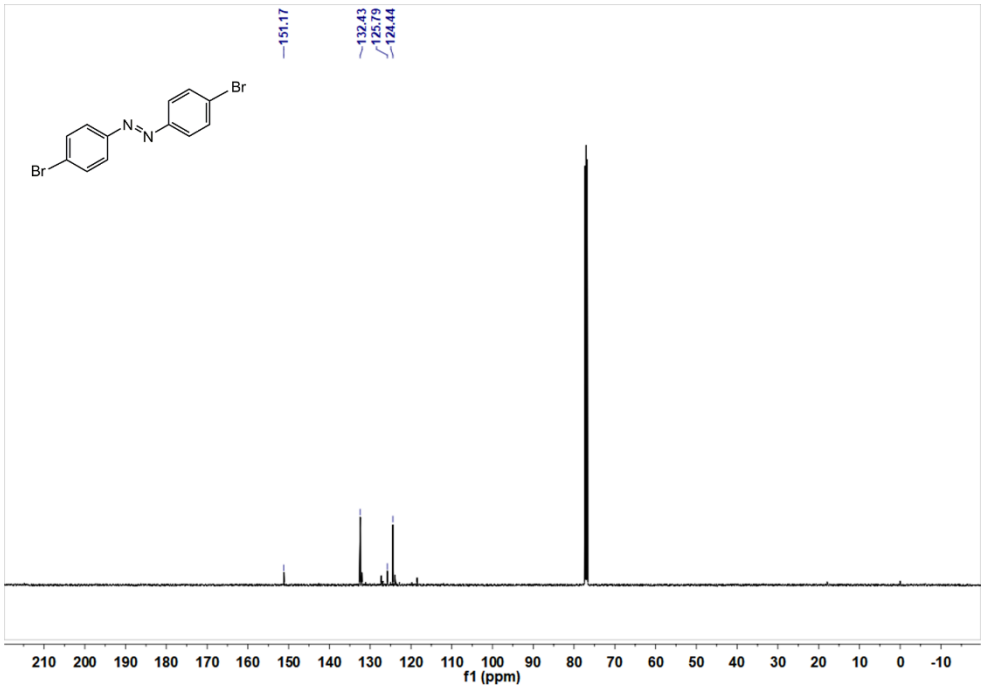

Fig. S59 ^{13}C NMR spectra of **3l** (126 MHz, $CDCl_3$).

(E)-1,2-bis(4-bromophenyl)diazene (3l): ^{13}C NMR (126 MHz, $CDCl_3$) δ 151.17 (s), 132.43 (s), 125.79 (s), 124.44 (s).

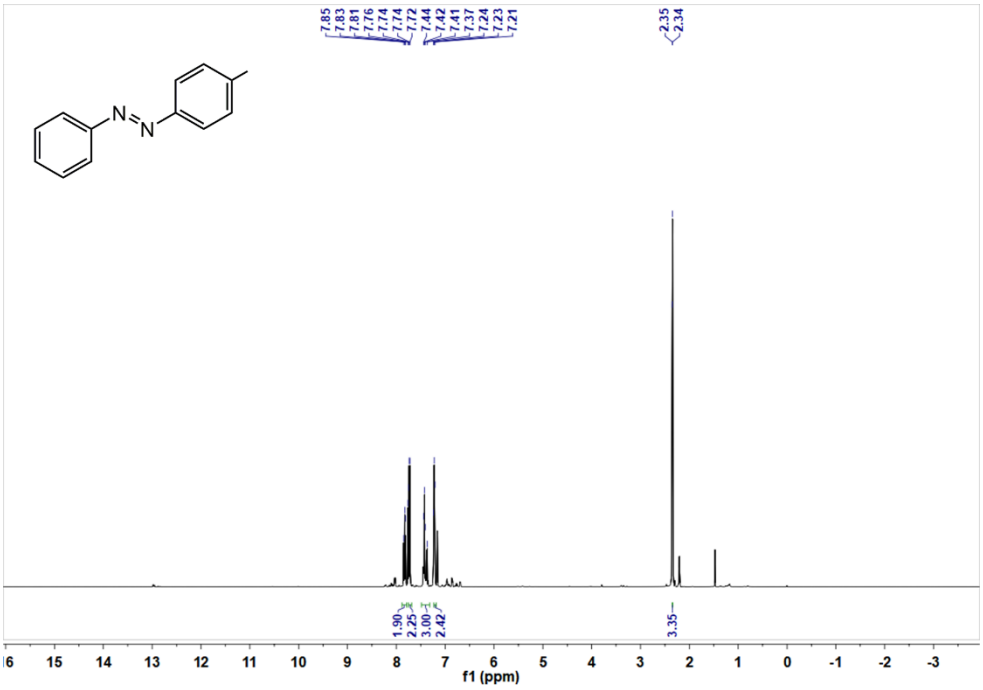

Fig. S60 ^{1}H NMR spectra of **3m** (500 MHz, $CDCl_3$).

(E)-1-(4-methylphenyl)-2-phenyldiazene (3m): ^{1}H NMR (500 MHz, $CDCl_3$) δ 7.89 – 7.79 (m, 2H), 7.75 – 7.69 (m, 2H), 7.41 (dd, J = 21.6, 13.8 Hz, 3H), 7.22 (d, J = 8.0 Hz, 2H), 2.35 (d, J = 3.7 Hz, 3H).

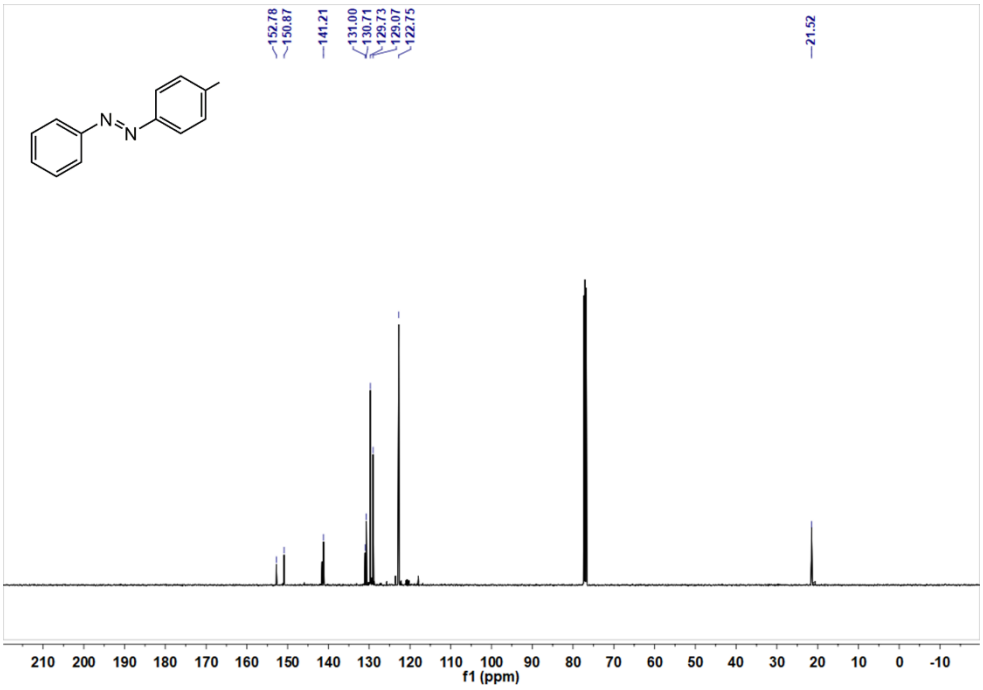

Fig. S61 ^{13}C NMR spectra of **3m** (126 MHz, $CDCl_3$).

(E)-1-(4-methylphenyl)-2-phenyldiazene (3m): ^{13}C NMR (126 MHz, $CDCl_3$) δ 152.78 (s), 150.87 (s), 141.21 (s), 131.00 (s), 130.71 (s), 129.73 (s), 129.07 (s), 122.75 (s), 21.52 (s).

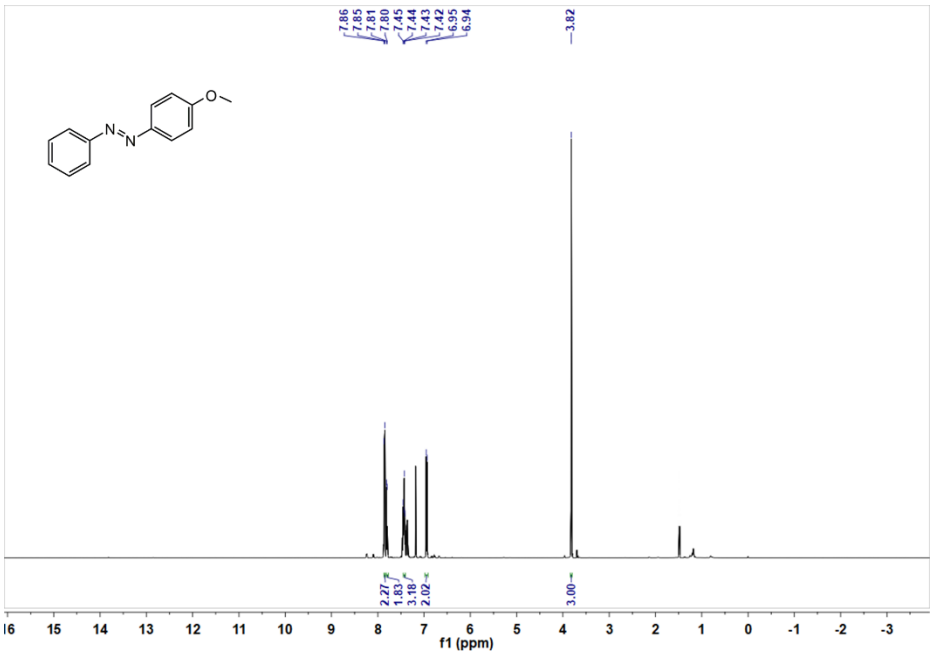

Fig. S62 ^{1}H NMR spectra of **3n** (500 MHz, $CDCl_3$).

(E)-1-(4-methoxyphenyl)-2-phenyldiazene (3n): ^{1}H NMR (500 MHz, $CDCl_3$) δ 7.85 (s, 2H), 7.81 (d, J = 7.2 Hz, 2H), 7.43 (t, J = 4.9 Hz, 3H), 6.94 (d, J = 9.0 Hz, 2H), 3.82 (s, 3H).

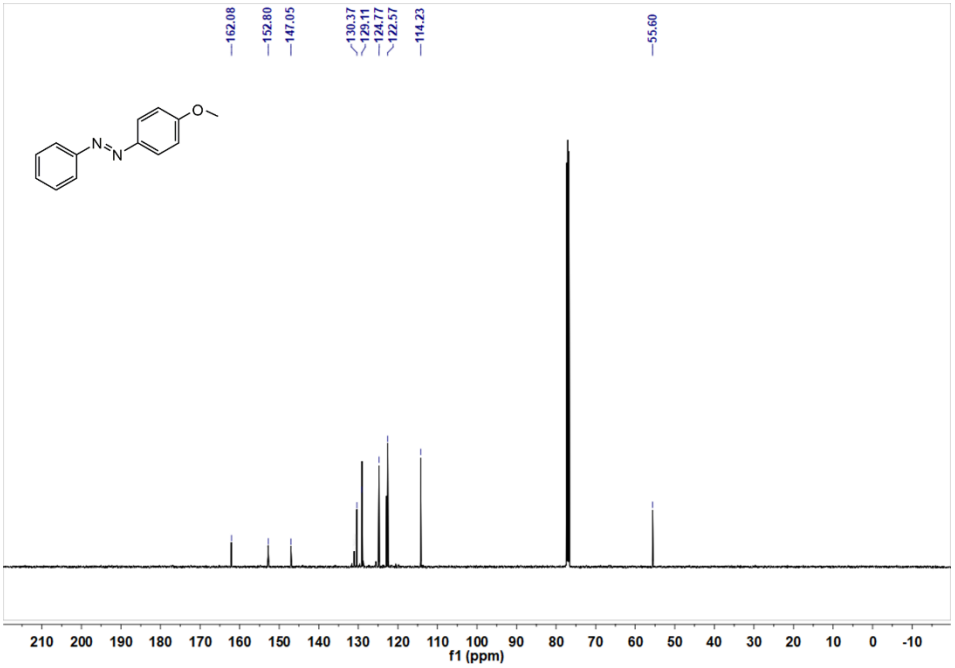

Fig. S63 ^{13}C NMR spectra of **3n** (126 MHz, $CDCl_3$).

(E)-1-(4-methoxyphenyl)-2-phenyldiazene (3n): ^{13}C NMR (126 MHz, $CDCl_3$)δ 162.08 (s), 152.80 (s), 147.05 (s), 130.37 (s), 129.11 (s), 124.77 (s), 122.57 (s), 114.23 (s), 55.60 (s).

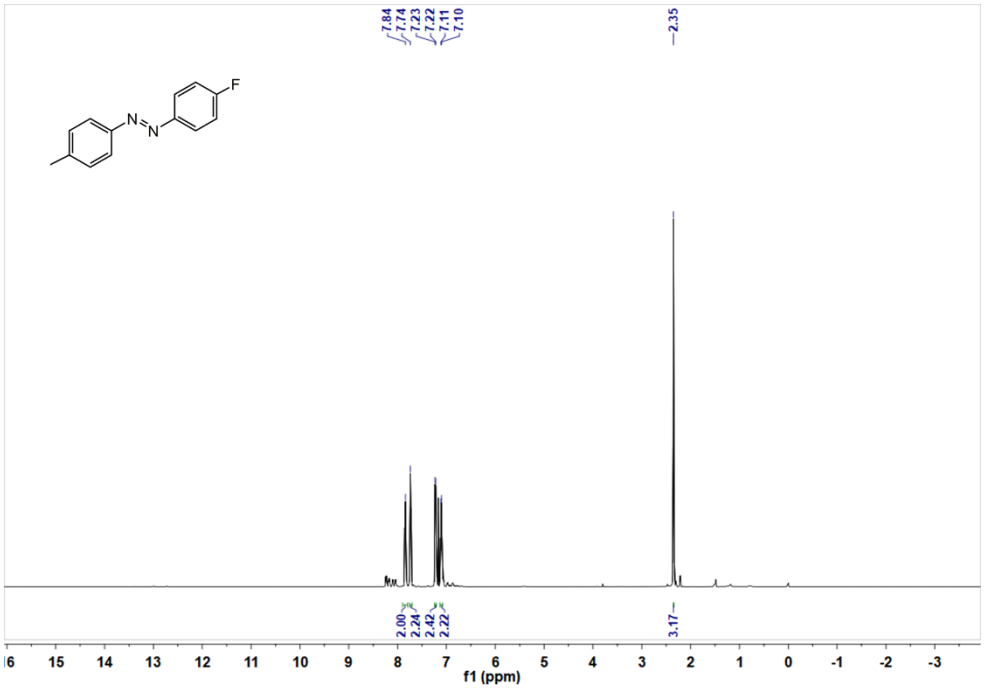

Fig. S64 ^{1}H NMR spectra of **3o** (500 MHz, $CDCl_3$).

(E)-2-(4-fluorophenyl)-1-(4-methylphenyl)diazene (3o): ^{1}H NMR (500 MHz, $CDCl_3$) δ 7.84 (s, 2H), 7.74 (s, 2H), 7.23 (d, J = 7.9 Hz, 2H), 7.11 (d, J = 4.0 Hz, 2H), 2.35 (s, 3H).

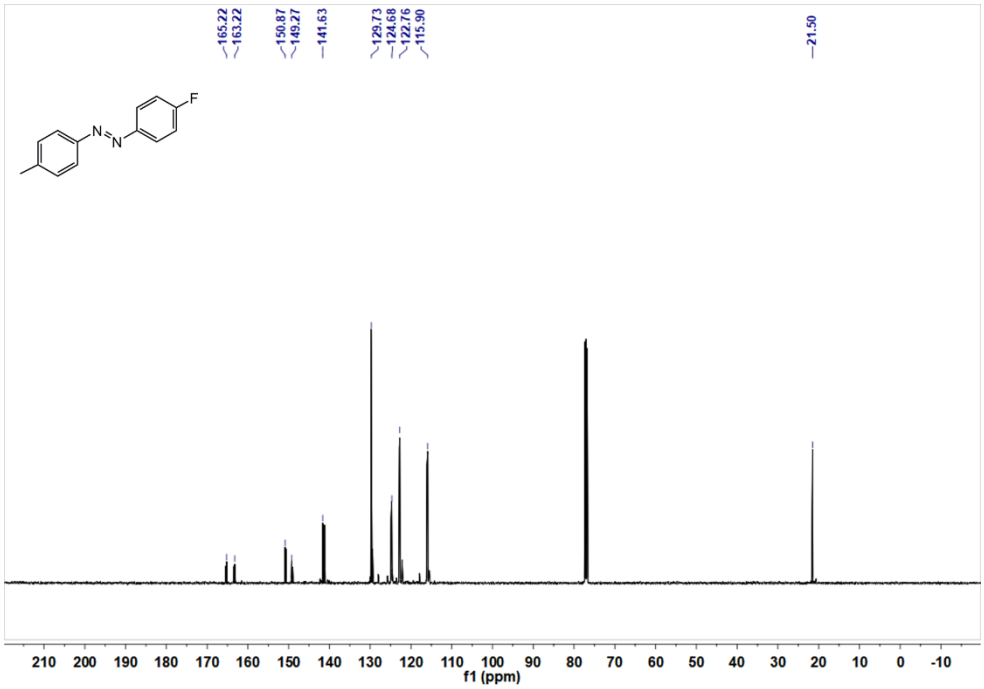

Fig. S65 ^{13}C NMR spectra of **3o** (126 MHz, $CDCl_3$).

(E)-2-(4-fluorophenyl)-1-(4-methylphenyl)diazene (3o): ^{13}C NMR (126 MHz, $CDCl_3$) δ 165.22 (s), 163.22 (s), 150.87 (s), 149.27 (s), 141.63 (s), 129.73 (s), 124.68 (s), 122.76 (s), 115.90 (s), 21.50 (s).

1 O. V. Dolomanov, L. J. Bourhis, R. J. Gildea, J. A. K. Howard and H. Puschmann, *J. Appl. Crystallogr.*, 2009, **42**, 339–341.
2 G. M. Sheldrick, *Acta Crystallogr., Sect. C: Struct. Chem.*, 2015, **71**, 3–8.
3 L. MacDonald, B. Rausch, M. D. Symes and L. Cronin, *Chem. Commun.*, 2018, **54**, 1093–1096.
4 T. H. Fleisch and G. J. Mains, *The Journal of Chemical Physics*, 1982, **76**, 780–786.
5 W. Feng, Y. Ding, Y. Liu and R. Lu, *Materials Chemistry and Physics*, 2006, **98**, 347–352.
6 Z. Xu, R. G. Palgrave and M. A. Hayward, *Inorg. Chem.*, 2020, **59**, 13767–13773.
7 M. Sheikhzadeh, S. Hejazi, S. Mohajernia, O. Tomanec, M. Mokhtar, A. Alshehri, S. Sanjabi, R. Zboril and P. Schmuki, *ChemCatChem*, 2019, **11**, 6258–6262.
8 C.-C. Nguyen, C.-T. Dinh and T.-O. Do, *RSC Adv.*, 2017, **7**, 3480–3487.
9 J. Kuncewicz and B. Ohtani, *RSC Adv.*, 2016, **6**, 77201–77211.
10 C. Ritchie, M. Speldrich, R. W. Gable, L. Sorace, P. Kögerler and C. Boskovic, *Inorg. Chem.*, 2011, **50**, 7004–7014.
11 H. Li, W. Chen, Y. Zhao, Y. Zou, X. Zhao, J. Song, P. Ma, J. Niu and J. Wang, *Nanoscale*, 2021, **13**, 8077–8086.
12 L.-P. Ji, J. Du, J.-S. Li, L.-C. Zhang, X.-J. Sang, H. Yang, H.-J. Cui and Z.-M. Zhu, *RSC Adv.*, 2016, **6**, 28956–28959.
13 R. Gupta, I. Khan, F. Hussain, A. M. Bossoh, I. M. Mbomekallé, P. de Oliveira, M. Sadakane, C. Kato, K. Ichihashi, K. Inoue and S. Nishihara, *Inorg. Chem.*, 2017, **56**, 8759–8767.
14 P. Ma, R. Wan, Y. Si, F. Hu, Y. Wang, J. Niu and J. Wang, *Dalton Trans.*, 2015, **44**, 11514–11523.
15 X.-J. Yang, M. Sun, H.-Y. Zang, Y.-Y. Ma, X.-J. Feng, H.-Q. Tan, Y.-H. Wang and Y.-G. Li, *Chem. – Asian J.*, 2016, **11**, 858–867.
16 X. Ma, K. Yu, J. Yuan, L. Cui, J. Lv, W. Dai and B. Zhou, *Inorg. Chem.*, 2020, **59**, 5149–5160.
17 W. Chen, H. Li, J. Song, Y. Zhao, P. Ma, J. Niu and J. Wang, *Inorg. Chem.*, 2022, **61**, 2076–2085.
18 F. Song, Y. Ding, B. Ma, C. Wang, Q. Wang, X. Du, S. Fu and J. Song, *Energy Environ. Sci.*, 2013, **6**, 1170.
19 X.-B. Han, Z.-M. Zhang, T. Zhang, Y.-G. Li, W. Lin, W. You, Z.-M. Su and E.-B. Wang, *J. Am. Chem. Soc.*, 2014, **136**, 5359–5366.
20 X.-B. Han, Y.-G. Li, Z.-M. Zhang, H.-Q. Tan, Y. Lu and E.-B. Wang, *J. Am. Chem. Soc.*, 2015, **137**, 5486–5493.
21 Y. Sheng, X. Wang, S. Yue, G. Cheng, X. Zou and X. Lu, *ChemCatChem*, 2020, **12**, 4632–4641.
22 Y. Xie, X. Shang, D. Liu, H. Zhao, Y. Gu, Z. Zhang and X. Wang, *Applied Catalysis B: Environmental*, 2019, **259**, 118087.
23 A. Kumar, B. Paul, R. Boukherroub and S. L. Jain, *Journal of Hazardous Materials*, 2020, **387**, 121700.
24 C. Yao, A. Yuan, Z. Wang, H. Lei, L. Zhang, L. Guo and X. Dong, *J. Mater. Chem. A*, 2019, **7**, 13071–13079.
25 B. Wang, Z. Deng and Z. Li, *Journal of Catalysis*, 2020, **389**, 241–246.
26 S. Han, Y. Cheng, S. Liu, C. Tao, A. Wang, W. Wei, H. Yu and Y. Wei, *Angew. Chem.*, 2021, **133**, 6452–6455.
27 J. Qin, Y. Long, F. Sun, P. Zhou, W. D. Wang, N. Luo and J. Ma, *Angew. Chem. Int. Ed.*, 2021, **60**, 2–9.
28 J. Jiao, H. Sun, C. Si, J. Xu, T. Zhang and Q. Han, *ACS Appl. Mater. Interfaces*, 2022, **14**, 16386–16393.
29 Y.-M. Lu, H.-Z. Zhu, W.-G. Li, B. Hu and S.-H. Yu, *J. Mater. Chem. A*, 2013, **1**, 3783–3788.
30 F. Tong, X. Liang, F. Ma, X. Bao, Z. Wang, Y. Liu, P. Wang, H. Cheng, Y. Dai, B. Huang and Z. Zheng, *ACS Catal.*, 2021, **11**, 3801–3809.
31 S. Füldner, P. Pohla, H. Bartling, S. Dankesreiter, R. Stadler, M. Gruber, A. Pfitzner and B. König, *Green Chem.*, 2011, **13**, 640–643.
32 P. Ji, K. Manna, Z. Lin, X. Feng, A. Urban, Y. Song and W. Lin, *J. Am. Chem. Soc.*, 2017, **139**, 7004–7011.
33 M. M. El-Masry, M. El-Shahat, R. Ramadan and R. M. Abdelhameed, *J Mater Sci: Mater Electron*, 2021, **32**, 18408–18424.
34 C. Liao, B. Liu, Q. Chi and Z. Zhang, *ACS Appl. Mater. Interfaces*, 2018, **10**, 44421–44429.
35 M. Tian, X. Cui, K. Liang, J. Ma and Z. Dong, *Inorg. Chem. Front.*, 2016, **3**, 1332–1340.
36 Y. Jang, S. Kim, S. W. Jun, B. H. Kim, S. Hwang, I. K. Song, B. M. Kim and T. Hyeon, *Chem. Commun.*, 2011, **47**, 3601–3603.
37 X.-J. Yang, B. Chen, L.-Q. Zheng, L.-Z. Wu and C.-H. Tung, *Green Chem.*, 2014, **16**, 1082–1086.
38 C. Zhang and N. Jiao, *Angew. Chem. Int. Ed.*, 2010, **49**, 6174–6177.
39 B. Dutta, S. Biswas, V. Sharma, N. O. Savage, S. P. Alpay and S. L. Suib, *Angew. Chem. Int. Ed.*, 2016, **55**, 2171–2175.
40 A. Grirrane, A. Corma and H. García, *Science*, 2008, **322**, 1661–1664.
41 A. Saha, S. Payra, B. Selvaratnam, S. Bhattacharya, S. Pal, R. T. Koodali and S. Banerjee, *ACS Sustainable Chem. Eng.*, 2018, **6**, 11345–11352.
42 S. Cai, H. Rong, X. Yu, X. Liu, D. Wang, W. He and Y. Li, *ACS Catal.*, 2013, **3**, 478–486.
43 F. Fu, S. He, S. Yang, C. Wang, X. Zhang, P. Li, H. Sheng and M. Zhu, *Sci. China Chem.*, 2015, **58**, 1532–1536.